A Hilbert Transform Sensitivity-based Model-Updating Method for Damage Detection of Structures with Closely-Spaced Eigenvalues

Sahar Hassani[a], Mohsen Mousavi[b], Amir H. Gandomi *[b]

[a] *Faculty of Engineering, Department of Civil Engineering, Ferdowsi University of Mashhad, Mashhad, Iran*
[b] *Faculty of Engineering and IT, University of Technology Sydney, Ultimo, NSW 2007, Australia*

Abstract

In this paper, a novel method is proposed for damage detection of structures with closely-spaced eigenvalues. The proposed method uses a transformed form of the condensed frequency response function matrix each of whose columns is obtained as the sum of the unwrapped instantaneous Hilbert phase of the corresponding decomposed column of the original matrix using Empirical Mode Decomposition (EMD) algorithm. A new sensitivity-based model updating equation is then developed which uses the constructed new matrix as input. The constructed sensitivity-based equation is solved via the least squares method through iterations to update unknown structural damage indices in an finite element model of the structure. To demonstrate the capability of the proposed method, the problem of damage detection in a composite laminate plate and a spatial truss structure, as examples of structures with closely-spaced eigenvalues, is solved. Moreover, the results obtained from the proposed method are compared against two other methods from the literature. The results show that the proposed method is far more effective at updating damage indices when incomplete highly noisy data is available.

Keywords: Damage identification, Hilbert transformation, Frequency response function, Composite laminate structures, optimisation algorithm, Closely-spaced eigenvalues

Email addresses: mohsen.mousavi@uts.edu.au (Mohsen Mousavi), gandomi@uts.edu.au (Amir H. Gandomi *)

Table 1: Damage identification levels.

Level	Label	Description
1	Detection	Detection of damage in structure
2	Localisation	Localisation of detected damage
3	Assessment	Quantification of damage severity
4	Prediction	Estimation of remaining service life

1. Introduction

Vibration-based damage detection methods can be categorised into three domains based on the type of vibration data used by these techniques. These are time domain, frequency domain, and time–frequency domain methods [1, 2]. In the time domain methods, time–history responses are directly used, whereas, in frequency domain methods, structural modal data is first derived out of a set of measured time history vibration data and are further used for damage detection. Time–frequency domain methods, however, are based on time–frequency analytical tools such as time-frequency signal decomposition algorithms [3].

The performance of damage detection methods is highly dependant on the choice of damage sensitive features. Model updating methods aim to modify some model property matrices such as mass, stiffness, and damping matrices to make the numerical predictions of the updated model compatible with those obtained from the real model. As such, any changes of the structural parameters can be referred to the presence of damage which can further lead to damage localisation and quantification (Levels 1–3 of damage identification in Table 1) [4].

Since the stiffness and mass matrices are assembled from all elements in the discrete finite element (FE) model, (1) the matrix properties of symmetry, sparseness and positive definiteness are guaranteed, (2) structural connectivity is preserved, and (3) changes in the updated global matrices are represented by changes in the updated parameters. Different structural responses such as FRFs, modal information, time histories, dynamic responses, strain responses, and a combination of static and modal test data have been used in model-updating problems [5]. Some model updating methods are based on sensitivity analysis of structural vibration data to the small variation of damage parameters. Sensitivity-based model updating methods aim at minimising a penalty function of errors obtained from the difference between the measured and simulated data [6]. These methods aim at measuring the changes in the model response due to a unit change in the model input which can be further used to characterise the sensitivity of the FE model parameters. In recent years, sensitivity-based methods have been given a great deal of attention due to their capability to reproduce measured responses robustly, through an updated analytical model.

Composite structures are widely used in different fields of engineering such as civil infrastructures, automotive and aerospace industry [7, 2]. These structures are, however, very prone to different failure

mechanisms either during the manufacturing process or whilst in service. These failure mechanisms include, but not limited to, fiber failure, matrix cracking, buckling, and delamination. These mechanisms have negative effects on the structural overall performance which can, in some cases, lead to catastrophic events. Therefore, developing new damage identification methods can bring about increasing the safety, efficiency, and service life of such structures as well as reducing their maintenance costs [8].

One limitation of using modal data for damage detection is the usage of only resonance modes for characterising structural vibration. Alternatively, using Frequency Response Functions (FRFs) reduce modal analysis errors stemming from closely-spaced resonances. Moreover, measured FRF data from vibration tests can better explain the structural dynamic behavior. Another advantage of using FRF, as opposed to the modal data, is that no pairing or matching of mode shapes is required. Therefore, new damage detection methods emerged based on the usage of FRFs [9, 10, 2].

It is known that the modal information of some complex structures such as composite laminates or 3D truss structures may be closely-spaced in some modes. Existence of such a phenomenon can result in a significant uncertainty in the structural response, making it difficult to perform damage detection of such structures. The modal data of such structures are highly sensitive to small changes in the mass or stiffness variations of the structure. This will make these data a bad choice as a damage sensitive feature (DSF) to be further used for damage detection [11]. Although FRFs have been used for damage detection of structures with closely-spaced eigenvalues by many researchers as a better alternative [12], these information are also very sensitive to measurement noise. Therefore, damage detection of such structures, using noisy FRF data, is still a challenge that needs to be addressed. One way to deal with this problem is to apply advanced signal processing techniques to come up with a signal that can capture variability in the FRF data due to damage even at the presence of high percentage of noise. Time-frequency signal processing approaches seek to identify a set of sub-signals extracted from an input signal for which two following assumptions hold: (1) the decomposed sub-signals are monocomponent, meaning that they contain only one mode of oscillation of the signal. Therefore, their frequency fluctuates within a narrow-band around their center frequency, and (2) the sum of the decomposed sub-signals construct the original signal. The first property of such sub-signals make the definition of instantaneous frequency, phase, and amplitude well-defined for them. Therefore, one can simply obtain the instantaneous properties of the original signal of interest through obtaining the sum of such properties taken over the decomposition results. Some of the most popular time-frequency signal processing approaches used for structural damage identification include: Wavelet transformation [13, 14], empirical mode decomposition (EMD) [15], ensemble empirical mode decomposition (EEMD) [16], Variational mode decomposition (VMD) [3]. These methods can be also used for denoising. This seems more crucial in damage detection of composite structures with closely-spaced eigenvalues [17, 18].

In this paper a novel sensitivity-based model-updating method is proposed for damage detection of structures with closely-spaced eigenvalues. The proposed method solves the problem of damage detection in one stage through updating a new objective function. The constructed objective function uses the sum of the Unwrapped Instantaneous Hilbert Phase (SUIHP) of the decomposed condensed FRF (CFRF) signal using the Empirical Mode Decomposition (EMD) algorithm [19]. We show that using the SUIHP of the CFRF brings about higher accuracy in the updated damage indices when the CFRF is contaminated with high percentage of noise. Next, the performance of the proposed method is compared against two other methods proposed in [20, 21]. Three performance criteria, namely relative error (RE), mean sizing error (MSE), and the closeness index (CI) are employed to evaluate the performance of the proposed method. This paper presents multiple novelties as listed below:

1. The problem of damage detection in two types of structures with closely-spaced eigenvalues, i.e. a laminated composite structure and a spatial truss structure, is solved through proposing a new sensitivity-based model updating method using incomplete noisy measurements.
2. A transformed form of the CFRF signal is used for robust damage detection of structures with closely-spaced eigenvalues. The new signal is obtained as the sum of the unwrapped instantaneous Hilbert Phase (SUIHP) of the decomposed CFRF signal employing the EMD algorithm.
3. A new approach for identifying the most suitable excitation locations for constructing CFRF signals, to be used for damage detection, is proposed based on the new transformed form of the CFRF signals.
4. The superiority of the proposed method is demonstrated through comparison with two other methods from the literature.

2. Proposing a new signal reconstruction based on CFRF signal

A new method is proposed in this paper for solving the damage detection problem of structures with closely-spaced eigenvalues. The proposed technique uses the condensed frequency response function (CFRF), but not in its normal form. The main aim is to obtain a new signal out of a CFRF signal which is believed to be more effective in mitigating the effect of noise on damage detection results. In this section, all theoretical backgrounds pertaining to obtaining such a new signal are discussed.

The proposed reconstructed signal is obtained through: (1) decomposing the CFRF signal using Empirical mode decomposition (EMD) algorithm, and (2) obtaining the Unwrapped Instantaneous Hilbert Phase (SUIHP) of the modes of the decomposed signal using the EMD algorithm (Figure 1). EMD is used to obtain a set of narrow-band oscillation modes from the CFRF signal termed as intrinsic mode functions (IMF). The UIHP of each IMF is well defined and can be obtained using Gabor's analytical

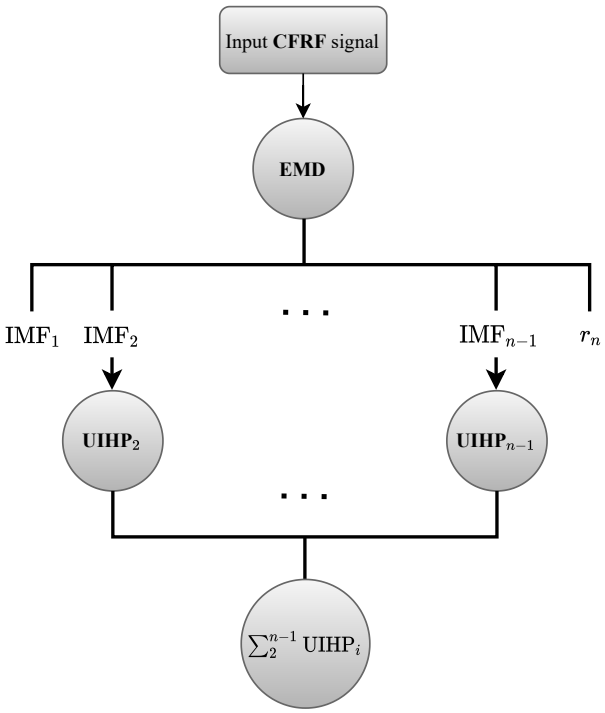

Figure 1: The flowchart of obtaining the proposed SUIHP.

signal as discussed in the following sections. Note that the first IMF (IMF_1) usually corresponds to the noise in the original signal and, therefore, is excluded from further analysis here. Likewise, the residual IMF r_n obtained from the decomposition process is also excluded from further analysis. Therefore, the sum of all UIHPs (SUIHP) of the decomposed signal, excluding IMF_1 and r_n, is introduced as the newly reconstructed signal.

The details of the decomposition process as well as the calculation of UIHP for each extracted IMF is discussed in the following sections.

2.1. Empirical mode decomposition (EMD)

The EMD algorithm, first introduced by Huang et al. [19], is a signal decomposition algorithm to be used to decompose a complex signal into its constructive oscillation modes, termed Intrinsic Mode Functions (IMFs). Unlike the Fourier basis, IMFs can be non-linear and/or non-stationary modulated signals. Based on the linear modal analysis, each IMF is a narrow-band signal (monocomponent) and is assumed to only involve one mode of oscillation of the original signal. Therefore, over short time windows, it can be regarded to be loosely sinusoidal in form. As such, the concepts of the instantaneous frequency, phase, and amplitude are well defined for the extracted IMFs.

The flowchart of the EMD algorithm applied to an CFRF signal is shown in Figure 2. One can decompose a signal in MATLAB (version 2018a onward) using the function `emd` as follows:

$$[\texttt{imf}, \texttt{residual}] = \texttt{emd}(\texttt{CFRF}); \tag{1}$$

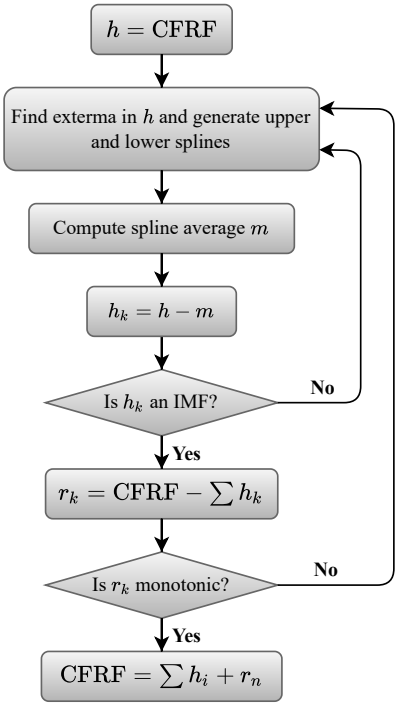

Figure 2: Flowchart of the EMD algorithm applied to a CFRF.

where `imf` is a matrix containing all the IMFs and `residual` is the vector of residuals. Since the first IMF_1 has the highest center frequency, it is deemed to correspond to noise in the signal (column of CFRF) and is thus excluded from further analysis in this study. Moreover, it is not a valid assumption to think of the residual IMF as the main trend of the original signal [22]. Hence, the residual IMF, r_n, is also excluded from further analysis to avoid any errors in the damage detection results.

2.2. Hilbert Transform

The Hilbert transform is widely used in modern signal processing to interpret signals. A signal needs to pass the causality condition for the Hilbert transform to be applied to it [23]. It means that the signal at any time is independent from any future events or conditions, implying that the value of the signal evaluated at a negative time is zero. The Hilbert transform of the causal signal $h(t)$ is its convolution with the signal $1/\pi t$ defined as follows:

$$\hat{h}(t) = \lim_{\epsilon \to 0} \frac{1}{\pi} \int_{|\tau - t| > \epsilon} \frac{h(\tau)}{t - \tau} \, d\tau, \tag{2}$$

where $\hat{h}(t)$ denotes the Hilbert Transform of the signal $h(t)$. Note that the limit in Eq.(2) satisfies Cauchy principle value for the integral [24]. It can be shown that the integral of Eq.(2) converges and thus the Hilbert transform is well-defined.

The analytic signal $h_a(t)$ is defined (see [25]) for further interpretation of instantaneous amplitude, frequency, and phase of a complex signal, the real and imaginary parts of which are the original signal

and its Hilbert transform, respectively. Therefore, one can write:

$$h_a(t) = h(t) + j\hat{h}(t). \tag{3}$$

Rewriting Eq.(3) using Euler's formula one obtains:

$$h_a(t) = h_m(t)\, e^{j\phi(t)}, \tag{4}$$

where $h_m(t)$ and $\phi(t)$ are respectively the time-variant "instantaneous amplitude" (IA) and "instantaneous phase" of the analytical signal $h_a(t)$ where

$$h_m(t) = \sqrt{h^2(t) + \hat{h}^2(t)}, \tag{5}$$

$$\phi(t) = \tan^{-1}\left(\frac{\hat{h}(t)}{h(t)}\right). \tag{6}$$

The continuous phase function is usually represented by unwrapped radian phases. As such, whenever the jump between consecutive angles is $\geq \pi$ radians, unwrap shifts the angles by adding multiples of $\pm 2\pi$ until the jump is less than π (see `unwrap` in MATLAB). Figure 3 visualises the above discussion, however, note that in case of having an CFRF signal, the x-axis is frequency as opposed to time. The unwrapped instantaneous Hilbert phase (UIHP) was shown to be informative about damage [26]. For instance, Pines and Salvino [27] demonstrated that the phase expression of structural vibration characteristics is sensitive to the variations in various structural parameters such as stiffness, mass, and damping. The authors proved that the Hilbert instantaneous phase is an effective damage sensitive feature. As such, it was anticipated that the phase expression would be a more effective damage sensitive feature in a simple one-dimensional structure. Here, this conclusion is tested as a hypothesis against damage detection of more complex structures. Moreover, it was shown in some previous attempts that the concept of instantaneous frequency (and, therefore, phase) can improve the physical meaningfulness of the IMFs extracted from the EMD algorithm [28]. This will further facilitate the process of damage detection. Moreover, the varying slope of the UIHP is hypothesized to be less sensitive to the measurement noise. Therefore, the UIHP of the structural response (IMFs obtained from the decomposed CFRF signal) is proposed to be used for damage detection.

Note that the definition of the instantaneous frequency, phase, and amplitude is well-defined only for narrow-band signals. Therefore, EMD needs to be first applied to the CFRF signal to extract its narrow-band IMFs, excluding IMF_1 and r_n, for which the UIHP is well defined. The sum of all UIHPs (SUIHP) is then used in the proposed model-updating based damage detection equation for updating damage indices. Note that, from now on, SUIHP refers to the new reconstructed signal from the input

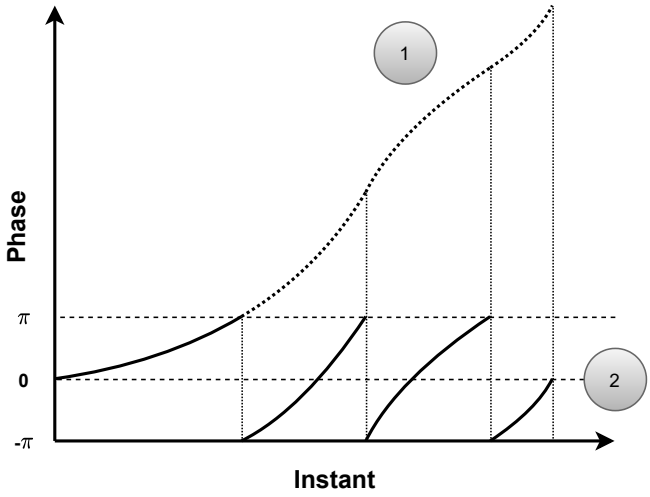

Figure 3: Instantaneous phase: (1) unwrapped, and (2) wrapped.

CFRF signal.

3. The proposed model-updating based damage detection methods using SUIHP

Model-updating methods aim at updating mass and stiffness matrices of structures using measured data. The simplified flowchart diagram of the model updating methods is shown in Figure 4.

Using FRF instead of modal data was recommended for damage detection of structures with closely-spaced eigenvalues [12]. The main reason is that modal data of such structures can suffer from the redundancy of information, stemming from closely-spaced modes. Therefore, selecting FRFs for damage detection of structures with closely-spaced eigenvalues seems reasonable. Moreover, since the proposed UIHP is less sensitive to noise it can further facilitate the process of damage detection in such structures at the presence of a high level of noise. Following, the details of the proposed damage detection method is presented.

3.1. Definition of CFRF

Consider a partitioned form of the stiffness, mass, and damping matrices of an FE model of a structure as follows:

$$K = \begin{bmatrix} K_{m\times m} & K_{m\times s} \\ K_{s\times m} & K_{s\times s} \end{bmatrix} \tag{7}$$

$$M = \begin{bmatrix} M_{m\times m} & M_{m\times s} \\ M_{s\times m} & M_{s\times s} \end{bmatrix} \tag{8}$$

$$C = \begin{bmatrix} C_{m\times m} & C_{m\times s} \\ C_{s\times m} & C_{s\times s} \end{bmatrix} \tag{9}$$

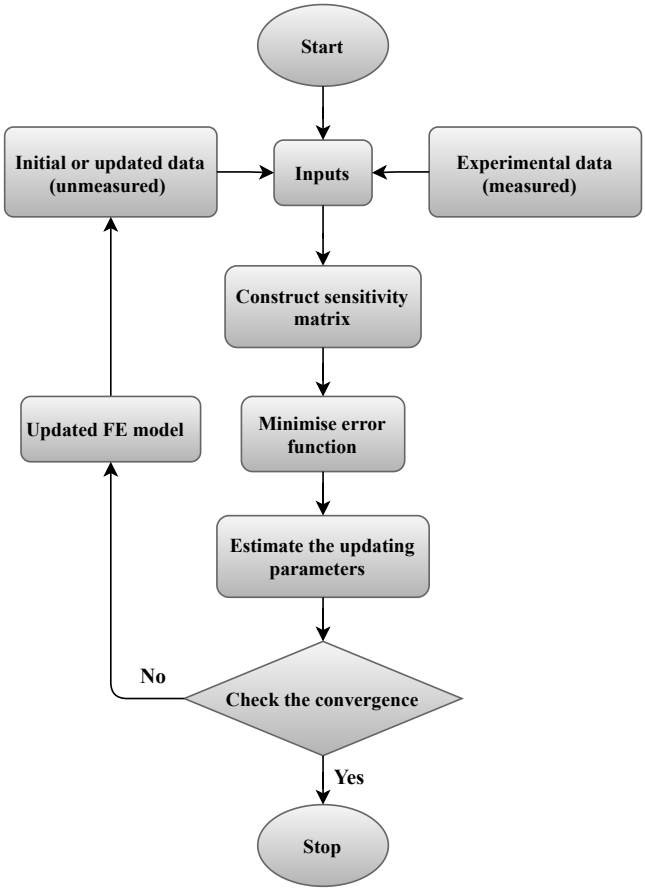

Figure 4: Simplified flowchart of the model-updating methods.

in which m and s represent respectively the number of master and slave degrees of freedom (DOFs). Considering rotational DOFs as slave DOFs, the translational DOFs are thus master DOFs. Using the static condensation transformation matrix T, one can condense the slave DOFs in Eq.(7) to Eq.(9) as follows [29]:

$$\bar{K} = T^{\mathrm{T}}\, K\, T \tag{10}$$

$$\bar{M} = T^{\mathrm{T}}\, M\, T \tag{11}$$

$$\bar{C} = T^{\mathrm{T}}\, C\, T \tag{12}$$

where $\bar{K}$, $\bar{M}$, and $\bar{C}$ denote, respectively, the condensed form of the stiffness, mass, and damping matrices. The complete CFRF matrix, shown as $\bar{H}$, is thus obtained as follows:

$$\bar{H}(\omega) = (-\omega^2 \bar{M} + j\omega\, \bar{C} + \bar{K})^{-1} \tag{13}$$

In practice, $\bar{H}$ is constructed by excitation and measurement conducted on master DOFs of the structure.

3.2. The proposed sensitivity-based damage detection method

Consider an n-DOF structure. The SUIHP of the CFRF is fed into a sensitivity-based model updating equation. In this section, the theoretical backgrounds of the proposed equation are discussed.

Consider a system excited at its masters DOFs by the force vector $\bar{F}(\omega_k)$, where ω_k denotes the k^{th} excitation frequency. The measured response of the structure at its masters DOFs with genuine parameter vector α can be written as follows:

$$\bar{X}_m\left(\alpha,\omega_k\right)=\bar{H}_m\left(\alpha,\omega_k\right)\bar{F}\left(\omega_k\right) \tag{14}$$

where $\bar{X}_{\mathrm{m}}\left(\alpha,\omega_k\right)$ is the measured structural response vector. Likewise, for a to-be-updated numerical FEM, one can write:

$$\bar{X}_c\left(\hat{\alpha},\omega_k\right)=\bar{H}_c\left(\hat{\alpha},\omega_k\right)\bar{F}\left(\omega_k\right) \tag{15}$$

where $\bar{X}_{\mathrm{c}}\left(\hat{\alpha},\omega_k\right)$ is the response vector of the FEM, $\hat{\alpha}$ is the estimated value of the vector of damage indices α, $\bar{H}_m\left(\alpha,\omega_k\right)$ and $\bar{H}_c\left(\hat{\alpha},\omega_k\right)$ are respectively the CFRFs obtained from the real and estimated models. As such, this estimation results in an error that is a function of $\hat{\alpha}$ and is defined as follows:

$$J\left(\hat{\alpha}\right)=\left\|\epsilon\right\|_2^2=\left\|\bar{X}_{\mathrm{m}}\left(\alpha,\omega_k\right)-\bar{X}_{\mathrm{c}}\left(\hat{\alpha},\omega_k\right)\right\|_2^2 \tag{16}$$

where $J\left(\hat{\alpha}\right)$ is the error function that depends on the estimated damage indices vector $\hat{\alpha}$, L^2 denotes the vector norm, and ϵ represents the residual vector. The approximated first-order Taylor series expansion of Eq.(16) is written as follows:

$$\bar{X}_{\mathrm{m}}\left(\alpha,\omega_k\right)\simeq\bar{X}_{\mathrm{c}}\left(\hat{\alpha},\omega_k\right)+\frac{\partial\bar{X}_{\mathrm{c}}\left(\hat{\alpha},\omega_k\right)}{\partial\hat{\alpha}}\,\delta\hat{\alpha} \tag{17}$$

Taking the derivative of the computed response vector $\bar{X}_{\mathrm{c}}\left(\hat{\alpha},\omega_k\right)$ with respect to $\hat{\alpha}$ results in the following equation [21]:

$$\begin{aligned}\frac{\partial\bar{X}_{\mathrm{c}}\left(\hat{\alpha},\omega_k\right)}{\partial\hat{\alpha}}&\simeq-\bar{H}_{\mathrm{c}}\left(\hat{\alpha},\omega_k\right)\\&\times\left(-\omega^2\frac{\partial\bar{M}}{\partial\hat{\alpha}}+j\omega\frac{\partial\bar{C}}{\partial\hat{\alpha}}+\frac{\partial\bar{K}}{\partial\hat{\alpha}}\right)\bar{X}_{\mathrm{c}}\left(\hat{\alpha},\omega_k\right)\end{aligned} \tag{18}$$

Substituting Eq.(18) into Eq.(17), we have:

$$\begin{aligned}\epsilon&=\bar{X}_{\mathrm{m}}\left(\alpha,\omega_k\right)-\bar{X}_{\mathrm{c}}\left(\hat{\alpha},\omega_k\right)\\&\simeq\Big[-\bar{H}_{\mathrm{c}}\left(\hat{\alpha},\omega_k\right)\left(-\omega^2\frac{\partial\bar{M}}{\partial\hat{\alpha}}+j\omega\frac{\partial\bar{C}}{\partial\hat{\alpha}}+\frac{\partial\bar{K}}{\partial\hat{\alpha}}\right)\\&\times\bar{X}_{\mathrm{c}}\left(\hat{\alpha},\omega_k\right)\Big]\,\delta\hat{\alpha}\end{aligned} \tag{19}$$

Eq.19 can be used to obtain $\hat{\alpha}$. Although neglecting the higher order of Taylor series expansion in Eq.(19) will result in an approximate solution, the negligence of those terms is expected not to compromise the precision of the final results. Writing the measured CFRF $\bar{H}_{\mathrm{m}}(\alpha, \omega_k)$ in terms of the perturbed structural stiffness, mass, and damping matrices, one obtains:

$$\bar{H}_{\mathrm{m}}(\alpha, \omega_k) = \left(-\omega^2(M + \delta M) + j\omega(C + \delta C) + K + \delta K\right)^{-1} \tag{20}$$

Eq.20 is employed to obtain the CFRF of the damaged structure for different values of ω_k [1]. The results of the different excitation frequencies are then concatenated to obtain a uniform CFRF. Note that the columns and rows of the CFRF correspond respectively to the excitation and measurement locations on the structure. Therefore, knowing the optimum excitation and measurement locations, the corresponding columns and rows of the obtained CFRF are selected (prior to the concatenation) to construct the final CFRF to be used for damage detection.

The Rayleigh damping model of the form $[C] = a[M] + b[K]$ was considered in Eq.(20). To this end, 5% damping ratio was considered for the two lowest modes of the structure to obtain a and b [30].

Hereafter, in order to develop the proposed damage detection, the effect of damping is neglected. Therefore, considering the terms corresponding to the stiffness and mass matrices and dropping the damping term in $\hat{\alpha}$, one can write:

$$\delta\bar{K} = \sum_{i=1}^{n} \frac{\partial \bar{K}}{\partial \hat{\alpha}_{\mathrm{i}}^{s}} \delta\hat{\alpha}_{\mathrm{i}}^{s} \tag{21}$$

$$\delta\bar{M} = \sum_{i=1}^{n} \frac{\partial \bar{M}}{\partial \hat{\alpha}_{\mathrm{i}}^{m}} \delta\hat{\alpha}_{\mathrm{i}}^{m} \tag{22}$$

where s and m indicate respectively parts of the matrix of damage parameters corresponding to the stiffness and mass matrices. The structural response variation of an undamped system in terms of the measured CFRF can be written in the following form [21]:

$$\begin{aligned} \delta\bar{X}_{\mathrm{c}}(\hat{\alpha}, \omega_k) \simeq & -\bar{H}_{\mathrm{m}}(\alpha, \omega_k) \\ & \times \left(-\omega_k^2 \delta\bar{M} + \delta\bar{K}\right) \bar{X}_{\mathrm{c}}(\hat{\alpha}, \omega_k) \end{aligned} \tag{23}$$

Substituting Eq.(21) and Eq.(22) into Eq.(23) and rewriting the obtained equation in a compact

[1] Note that, in this paper, damage is simulated as a degradation introduced to the stiffness matrix of structure. Therefore, the terms δM and δC, in Eq.(20), were neglected in simulations.

form results in the following equation:

$$\delta\bar{X}(\hat{\alpha},\omega_k) \simeq \begin{bmatrix} \bar{S}^s & \bar{S}^m \end{bmatrix} \begin{bmatrix} \delta\hat{\alpha}^s \\ \delta\hat{\alpha}^m \end{bmatrix} \tag{24}$$

where

$$\bar{S}^s = \Big[-\bar{H}_{\mathrm{m}}(\alpha,\omega_k)\left(\frac{\partial\bar{K}}{\partial\hat{\alpha}_1^s}\right)\bar{X}_{\mathrm{c}}(\hat{\alpha},\omega_k), \ldots, -\bar{H}_{\mathrm{m}}(\alpha,\omega_k)\left(\frac{\partial\bar{K}}{\partial\hat{\alpha}_n^s}\right)\bar{X}_{\mathrm{c}}(\hat{\alpha},\omega_k)\Big] \tag{25}$$

and

$$\bar{S}^m = \Big[-\bar{H}_{\mathrm{m}}(\alpha,\omega_k)\left(\frac{\partial\bar{M}}{\partial\hat{\alpha}_1^m}\right)\bar{X}_{\mathrm{c}}(\hat{\alpha},\omega_k), \ldots, -\bar{H}_{\mathrm{m}}(\alpha,\omega_k)\left(\frac{\partial\bar{M}}{\partial\hat{\alpha}_n^m}\right)\bar{X}_{\mathrm{c}}(\hat{\alpha},\omega_k)\Big] \tag{26}$$

Note that the SUIHP of the CFRF, shown as $\tilde{H}(\alpha,\omega_k)$, is substituted for $\bar{H}(\alpha,\omega_k)$ in Eq.(25) and Eq.(26). Also, in this paper, it is assumed that damage can only modify the stiffness matrix of the structure. Therefore, Eq.(24), Eq.(25), and Eq.(26) can be written as follows:

$$\delta\tilde{X}(\hat{\alpha},\omega_k) \simeq \tilde{S}^s \ \delta\hat{\alpha}^s \tag{27}$$

where

$$\tilde{S}^s = \Big[-\tilde{H}_{\mathrm{m}}(\alpha,\omega_k)\left(\frac{\partial\bar{K}}{\partial\hat{\alpha}_1^s}\right)\bar{X}_{\mathrm{c}}(\hat{\alpha},\omega_k), \ldots, -\tilde{H}_{\mathrm{m}}(\alpha,\omega_k)\left(\frac{\partial\bar{K}}{\partial\hat{\alpha}_n^s}\right)\tilde{X}_{\mathrm{c}}(\hat{\alpha},\omega_k)\Big] \tag{28}$$

Considering Eq.(14) and Eq.(15), one can obtain $\delta\tilde{X}(\hat{\alpha}^s,\omega_k)$ as follows:

$$\delta\tilde{X}(\hat{\alpha}^s,\omega_k) = \underbrace{\tilde{H}_m\left(\alpha^s,\omega_k\right)\bar{F}\left(\omega_k\right)}_{\tilde{X}_m(\alpha^s,\omega_k)} - \underbrace{\tilde{H}_c\left(\hat{\alpha}^s,\omega_k\right)\bar{F}\left(\omega_k\right)}_{\tilde{X}_c(\hat{\alpha}^s,\omega_k)} \tag{29}$$

Therefore,

$$\delta\hat{\alpha}^s \simeq \left(\tilde{S}^s\right)^+ \left(\tilde{H}_m\left(\alpha^s,\omega_k\right)\bar{F}\left(\omega_k\right) - \tilde{H}_c\left(\hat{\alpha}^s,\omega_k\right)\bar{F}\left(\omega_k\right)\right) \tag{30}$$

where superscript $+$ represents the Moore–Penrose inverse that obtains the inverse of a non-square matrix [30]. The least squares (LS) method is employed to solve Eq.(30) in iterations. As such, the value of $\hat{\alpha}^s$ at the t^{th} iteration is updated as $\hat{\alpha}_t^s = \hat{\alpha}_{t-1}^s + \delta\hat{\alpha}_t^s$. The convergence criteria for the algorithm was set as $|\delta\hat{\alpha}_t| \leq 10^{-5}$. Since the SUIHP of the CFRF is relatively a slowly varying function compared with CFRF, a larger number of iterations may be required for Eq.(30) to converge to a solution. The steps of the proposed algorithm can be presented as follows:

1. Initialize $\hat{\alpha}$ as a vector of zeros.
2. Obtain $\tilde{S}^{\bar{K}}$ from Eq.(28), given $\tilde{H}_{\mathrm{m}}(\alpha,\omega_k)$ as input, and $\bar{X}_{\mathrm{c}}(\hat{\alpha},\omega_k) = \tilde{H}_c\left(\hat{\alpha}^s,\omega_k\right)\bar{F}\left(\omega_k\right)$.
3. Compute $\delta\hat{\alpha}^s$ from Eq.(30) at each iteration to update $\hat{\alpha}_t^s = \hat{\alpha}_{t-1}^s + \delta\hat{\alpha}_t^s$.
4. Repeat steps (2) and (3) and check for the convergence criteria, i.e. $|\delta\hat{\alpha}_t| \leq 10^{-5}$.

4. The effective arrangement of the excitation frequency ranges and proposed locations

Choosing an appropriate frequency range plays an important role in CFRF-based model updating methods in order to achieve better results. As such, frequency ranges with higher sensitivity to the variations of the structural parameters are preferred. Previous studies revealed that the excitation frequency ranges near resonances serve this purpose well [31]. This is because of the two important features of such frequency ranges as follows:

1. The structural response in such frequency ranges is more sensitive to small variation of the structural parameters, and
2. Measurement noise in these ranges has less effect on damage detection results.

Reiterated, in this paper, damping is not considered to be updated. However, its effect on updating other parameters is considered, although it is desirable to diminish these effects as much as possible. It is known that the effect of damping on CFRF reduces drastically by staying away from resonances. Therefore, the excitation frequency ranges are considered to be far enough from resonances, although this distance needs to be adjusted case-wise. This will result in having CFRF signals obtained from different frequency ranges. The obtained CFRF signals are then concatenated to obtain a uniform signal. This will prevent the nonlinear variations of the CFRF, resulting in a uniform reduction of the response residual vector during the optimisation process. Note that since the damage indices are updated in each iteration, the computed CFRF signal $H_c(\omega)$ corresponding to the analytical model shifts slightly at each iteration. Therefore, $H_c(\omega)$ needs to be updated at each iteration as well. This is done through an automated frequency-range-selection program based on the aforementioned rules at each iteration.

The structure can be excited in different ways such as: (1) by a short impulse, (2) by applying a stepped sine excitation over the frequency range of interest, and (3) using a white noise or pseudo random noise. Note that the driving force, in a real experiment, is usually applied by a shaker. In the case of impact testing, though, it is usually applied by an instrumented hammer. It is generally known that the proper selection of the excitation locations can bring about more accurate results regarding the calculation of damage indices through solving the optimisation problem [32].

Proper selection of the excitation locations secures accurate results for a model-updating approach based on CFRFs. Therefore, in this section, an efficient method is proposed for obtaining optimum locations (DOFs) for exciting the structure to obtain its CFRFs. Note that, it is not desirable to have rotational DOFs among such locations when it comes to excite a composite plate structure. The proposed equation is based on the following equation presented in [33]:

$$\Lambda = \sum_{k=1}^{nf} \sqrt{\sum_{i=1}^{n} \left(H_{ij}(\omega_k)\right)^2} \tag{31}$$

where H is the complete FRF of the structure. Here, the optimum excitation locations are proposed to be selected based on the second norm of the summation of all rows of $\tilde{H}$ in the selected excitation frequency range. The optimum excitation locations are thus obtained at the ne highest values of the entries of $\tilde{\Lambda}$ with maximum values as defined in the following equation:

$$\tilde{\Lambda} = \sum_{k=1}^{N} \sqrt{\sum_{i=1}^{n} \left(\tilde{H}_{ij}(\omega_k)\right)^2} \tag{32}$$

According to Section 4, a proper excitation frequency range, i.e. an excitation range distg... ant enough from the resonance frequencies of the structure, makes the damping ineffective. Note that thus a frequency range around the first natural frequency of the structure is only used as the excitation frequency range in this paper. Moreover, it is worth mentioning that the optimum excitation locations are obtained based on the available FE model of the intact structure and, therefore, do not need to be updated at each iteration. This also makes sense from the practical point of view.

5. Damage identification accuracy indicators

In order to characterise the errors of the proposed method in updating damage indices, different indicators, adopted from [34], are employed as follows:

1. The closeness index (CI) is used to evaluate and compare the accuracy of the predicted damage indices. It is defined based on the difference between the actual and the obtained structural parameters vectors as follows:

$$\mathrm{CI} = 1 - \frac{\|P_e^r - P_e^c\|_2}{\|P_e^r\|_2} \tag{33}$$

   where P_e^r and P_e^c represent respectively the vectors of the real and computed damage indices. As such, all the updated parameters are exact when CI = 1.

2. The mean sizing error (MSE) is defined as the mean value of the absolute variations between the real elemental parameter p_e^r and the computed elemental parameter p_e^c summed over all the defective elements. Therefore, MSE, over the de number of located damaged elements, is defined as follows:

$$\mathrm{MSE} = \frac{1}{de} \sum_{e=1}^{de} |p_e^r - p_e^c|, \quad 0 \leq \mathrm{MSE} \tag{34}$$

3. The relative error (RE) is defined as follows:

$$\mathrm{RE} = \frac{\sum_{e=1}^{de} |p_e^r| - \sum_{e=1}^{de} |p_e^c|}{\sum_{e=1}^{de} |p_e^c|}, \quad -1 \leq \mathrm{RE} \leq 1 \tag{35}$$

   Where the smaller value of MSE and RE implies more accurate predictions.

Table 2: The material properties of each ply in the composite laminate plate adopted from [35].

Young's Modulus	Young's Modulus	Poisson ratio	Poisson ratio	Modulus of rigidity	Modulus of rigidity
E_1 $(\mathrm{N/m^2})$=40	E_2 $(\mathrm{N/m^2})$=1	ν_{12}=0.25	ν_{21}=0.00625	$G_{12} = G_{13} = 0.6E_2$	$G_{23} = 0.5E_2$

Table 3: Damage scenarios of the composite laminate plate.

Case 1		Case 2		Case 3		Case 4		Case 5		Case 6	
Element	Ratio	Element	Ratio	Element	Ratio	Element	Ratio	Element	Ratio	Element	Ratio
5	0.20	2	0.15	1	0.20	5	0.15	4	0.15	3	0.20
12	0.30	10	0.20	10	0.15	10	0.10	8	0.20	7	0.15
24	0.15	15	0.25	12	0.10	15	0.20	17	0.30	9	0.10
31	0.20	25	0.30	13	0.20	20	0.25	23	0.15	19	0.30
		31	0.20	17	0.30	25	0.30	31	0.10	23	0.35
				29	0.25	30	0.10	36	0.20	31	0.20

6. Numerical examples

6.1. Laminated composite model

A fixed supported square composite plate, adopted from [35], with different number of layers (NoL) and layering angles (LA) is studied in this section. The plate, of the size $100 \times 100 \times 10$ cm, is divided into $n_x \times n_y$ four-node elements with a total number of $(n_x+1)\times(n_y+1)$ nodes (as shown in Figure 6a), where n_x and n_y denote respectively the number of divisions through the x and y axes (Figure 6b). Therefore, the plate is divided into 36 elements resulting in having 245 DOFs, including three translational and two rotational DOFs at each node. Since the four sides of the plate are fixed, 125 DOFs remain active. The material properties of the plate is listed in Table 2. In order to demonstrate the capability of the proposed method in damage detection of different configurations of the plate, several damage scenarios are considered. Table 3 shows six different damage scenarios based on the location, severity, and the type of damage. Damage is considered as a degradation factor introduced to the elemental stiffness (stiffness reduction). All the FE models of the simulated structures as well as damage detection algorithm were coded in an in-house Matlab software. The first-order shear deformation theory (FSDT)—an extended version of the classical laminated plate theory (CLPT) [35]—was employed for the simulation of the laminated composite plates in this study.

The 10 lowest natural frequencies of the healthy and damaged composite laminate plates with different configurations, considering different damage scenarios, are listed in Table 4. Accordingly, it is clear that reducing the stiffness results in decreasing the natural frequencies in all the studied models.

It is well understood that structures with many DOFs, such as spatial truss and plate structures, exhibit closely-spaced eigenvalues phenomenon [36]. However, the existence of such a phenomenon results in missing information about damage due to having redundant information stemming from the repeated modes. As a result, more information from higher modes has to be extracted to compensate for the redundant information from lower repeated modes. However, measuring higher modes is usually

Table 4: First ten natural frequencies of the composite laminate plate with different NoL and LA, in Hz.

Lamination scheme		Mode No.									
		1	2	3	4	5	6	7	8	9	10
Intact	NoL = 3, LA = (0°/90°/0°)	7.40	11.14	14.32	16.23	18.74	21.42	23.32	23.90	25.74	26.29
	NoL = 6, LA = (0°/45°/0°/0°/45°/0°)	7.64	11.53	14.74	16.82	19.07	21.99	23.78	24.90	25.78	26.60
Case 1	NoL = 3, LA = (0°/90°/0°)	7.30	11.01	14.11	15.92	18.61	21.08	23.08	23.58	25.39	25.92
	NoL = 6, LA = (0°/45°/0°/0°/45°/0°)	7.55	11.42	14.55	16.48	19.01	21.53	23.54	24.68	25.46	26.40
Case 2	NoL = 3, LA = (0°/90°/0°)	7.32	10.94	14.07	15.85	18.44	21.03	22.95	23.42	25.34	25.89
	NoL = 6, LA = (0°/45°/0°/0°/45°/0°)	7.55	11.34	14.50	16.45	18.74	21.50	23.41	24.53	25.44	26.31
Case 3	NoL = 3, LA = (0°/90°/0°)	7.24	10.96	14.03	15.96	18.50	21.03	22.73	23.47	25.26	25.79
	NoL = 6, LA = (0°/45°/0°/0°/45°/0°)	7.47	11.33	14.45	16.55	18.82	21.54	23.26	24.42	25.31	26.02
Case 4	NoL = 3, LA = (0°/90°/0°)	7.27	10.94	14.06	15.85	18.46	21.01	22.80	23.43	25.34	25.88
	NoL = 6, LA = (0°/45°/0°/0°/45°/0°)	7.52	11.33	14.49	16.41	18.83	21.48	23.28	24.50	25.42	26.31
Case 5	NoL = 3, LA = (0°/90°/0°)	7.28	10.99	14.22	16.06	18.45	21.05	22.92	23.61	25.33	25.85
	NoL = 6, LA = (0°/45°/0°/0°/45°/0°)	7.52	11.35	14.63	16.62	18.80	21.61	23.40	24.54	25.39	26.14
Case 6	NoL = 3, LA = (0°/90°/0°)	7.19	10.94	13.95	15.92	18.43	20.99	22.67	23.50	25.10	25.80
	NoL = 6, LA = (0°/45°/0°/0°/45°/0°)	7.43	11.29	14.40	16.51	18.68	21.67	23.18	24.37	25.19	25.98

more challenging. Therefore, damage detection of such structures is relatively a more challenging task [17, 37, 18].

A metric is introduced here to characterise the extent of the close-modes phenomenon in an undamped structure, which is based on a similar concept introduced in [17, 18] for damped structures. As such, two eigenvalues with the frequencies $\omega_1 = \omega$ and $\omega_2 = \omega + \Delta\omega$ are considered closely-spaced if $\Delta\omega = \omega_2 - \omega_1$ is distinctively small compared to ω [37]. As such, the frequency relative disparity index (FRD), for two adjacent frequencies (i, j) is introduced as follows:

$$\mathrm{FRD}_{i,j}\% = \left| \frac{f_j - f_i}{f_i} \right| \times 100 \tag{36}$$

where $f_j = \omega_j/2\pi$ and $f_i = \omega_i/2\pi$ are respectively the jth and ith natural frequencies in Hz. Intuitively, two modes are considered "well-separated" when $\mathrm{FRD}_{i,j} > 10\%$, "separated" when $5\% < \mathrm{FRD}_{i,j} \leq 10\%$, "close" when $1\% < \mathrm{FRD}_{i,j} \leq 5\%$, and "very close" when $\mathrm{FRD}_{i,j} \leq 1\%$ [17].

Figure 7 shows the closely-spaced eigenvalues characterisation of the composite laminate plate with different configurations. As can be seen from the figure, a number of resonances are closely-spaced (marked zones). Table 5 presents the obtained FRF for the first ten modes. As clarified earlier, model updating of structures with large number of unknowns and closely-spaced modes is a challenging task.

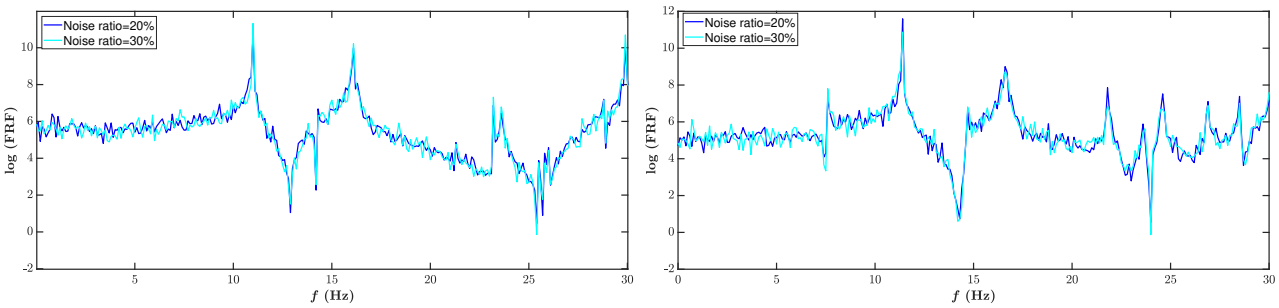

(a) NOL = 3 and LA = $(0°/90°/0°)$ and $n_x = n_y = 6$ (b) NOL = 6, LA = $(0°/45°/0°/0°/45°/0°)$, $n_x = n_y = 6$

Figure 5: The obtained noisy FRF signal corresponding to the composite laminate plate with different arrangements (for the 1st damage scenario, excited at DOF 21 and measured at DOF 72).

This is thus correct for the problem of damage detection in the laminated composites of this paper.

The error in damage detection will further increase when the modal and FRF data is highly contaminated with noise. Therefore, different level of noise was introduced to the modal and FRF data as discussed in the following section.

6.2. Considering the effect of noise

Using data contaminated with measurement noise can ruin the results of the damage detection. Therefore, it is vital to investigate the effect of measurement noise on the performance of the proposed damage detection method. To this end, the simulated structural FRF data were contaminated with different noise level using the following formula [38]:

$$\hat{\delta} = \delta + \frac{\mathrm{NP}}{100}\, n_{noise}\, \sigma(\delta) \tag{37}$$

where δ and $\hat{\delta}$ are respectively a simulated column of clean and noisy FRF data with standard deviation $\sigma(\delta)$, where NP is the noise percentage (20 and 30). Finally, n_noise is a vector of random variables sampled from a standard normal distribution.

Figure 5 displays examples of the obtained noisy FRF signals obtained from the composite laminate plate with different configurations.

6.3. The selection of measurement locations

The way of selecting DOFs to be measured for constructing CFRF has a great effect on the damage detection results. We mark the three translational DOFs of an element in all of its nodes as DOFs_t^1, DOFs_t^2, and DOFs_t^3 in the global coordinates. Figure 8 shows the obtained $\tilde{H}(f)$ for the intact and damaged structures calculated from the concatenated CFRF signals computed from different excitation frequency ranges within the first ten modes.[2] The obtained results regarding the 4th damage scenario

[2]Note that $f = \omega/2\pi$.

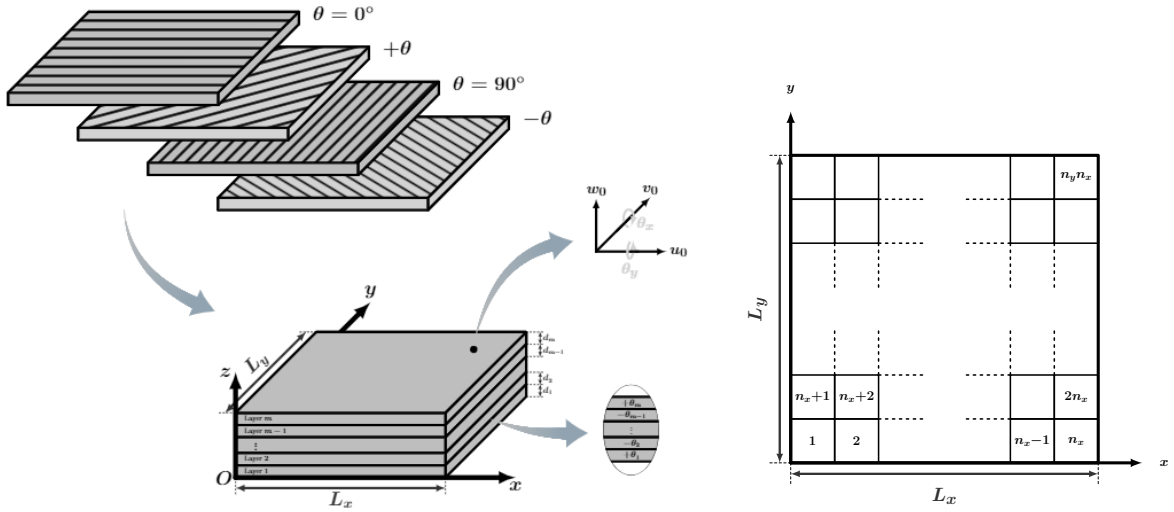

(a) (b)

Figure 6: (a) The sketch of the composite laminate plate. (b) Element numbering of the composite laminate plate ($n_x = n_y = 6$) [39].

Table 5: The $FRD_{i,j}$ values for the first ten modes of the composite laminate plate with different NOL and LA and $n_x = n_y = 6$.

Mode No.	Closely spaced modes with lamination scheme			
	NoL = 3, LA = (0°/90°/0°)		NoL = 6, LA = (0°/45°/0°/0°/45°/0°)	
	$FRD_{i,j}$ (%)	Modal disparity	$FRD_{i,j}$ (%)	Modal disparity
[1, 2]	50.54	Well-separated	50.92	Well-separated
[2, 3]	28.55	Well-separated	27.84	Well-separated
[3, 4]	13.33	Well-separated	14.11	Well-separated
[4, 5]	15.46	Well-separated	13.37	Well-separated
[5, 6]	14.30	Well-separated	15.31	Well-separated
[6, 7]	8.87	Separated	8.40	Separated
[7, 8]	2.48	Close	4.70	Close
[8, 9]	7.69	Separated	3.49	Close
[9, 10]	2.14	Close	3.22	Close
[10, 11]	12.00	Well-separated	1.69	Close

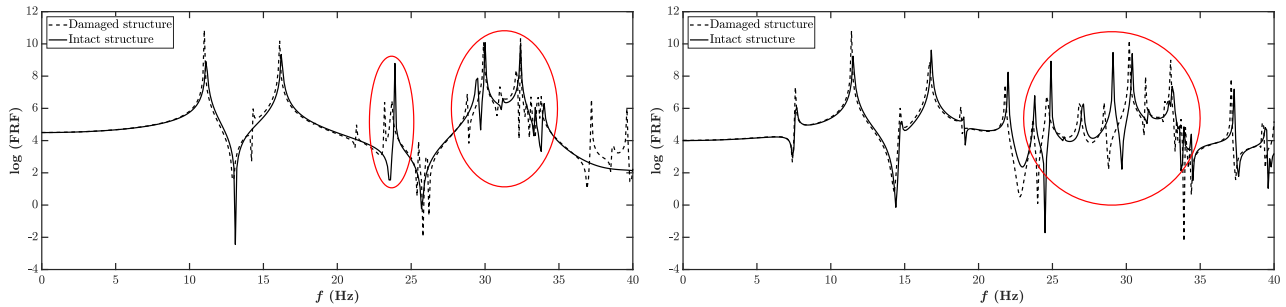

(a) NoL = 3 and LA = (0°/90°/0°) and $n_x = n_y = 6$ (b) NoL = 6, LA = (0°/45°/0°/0°/45°/0°), $n_x = n_y = 6$

Figure 7: The closely-spaced natural frequencies of the intact and damaged composite laminate plate with different arrangements (damage scenario 1, excited at DOF 21 and measured at DOF 12).

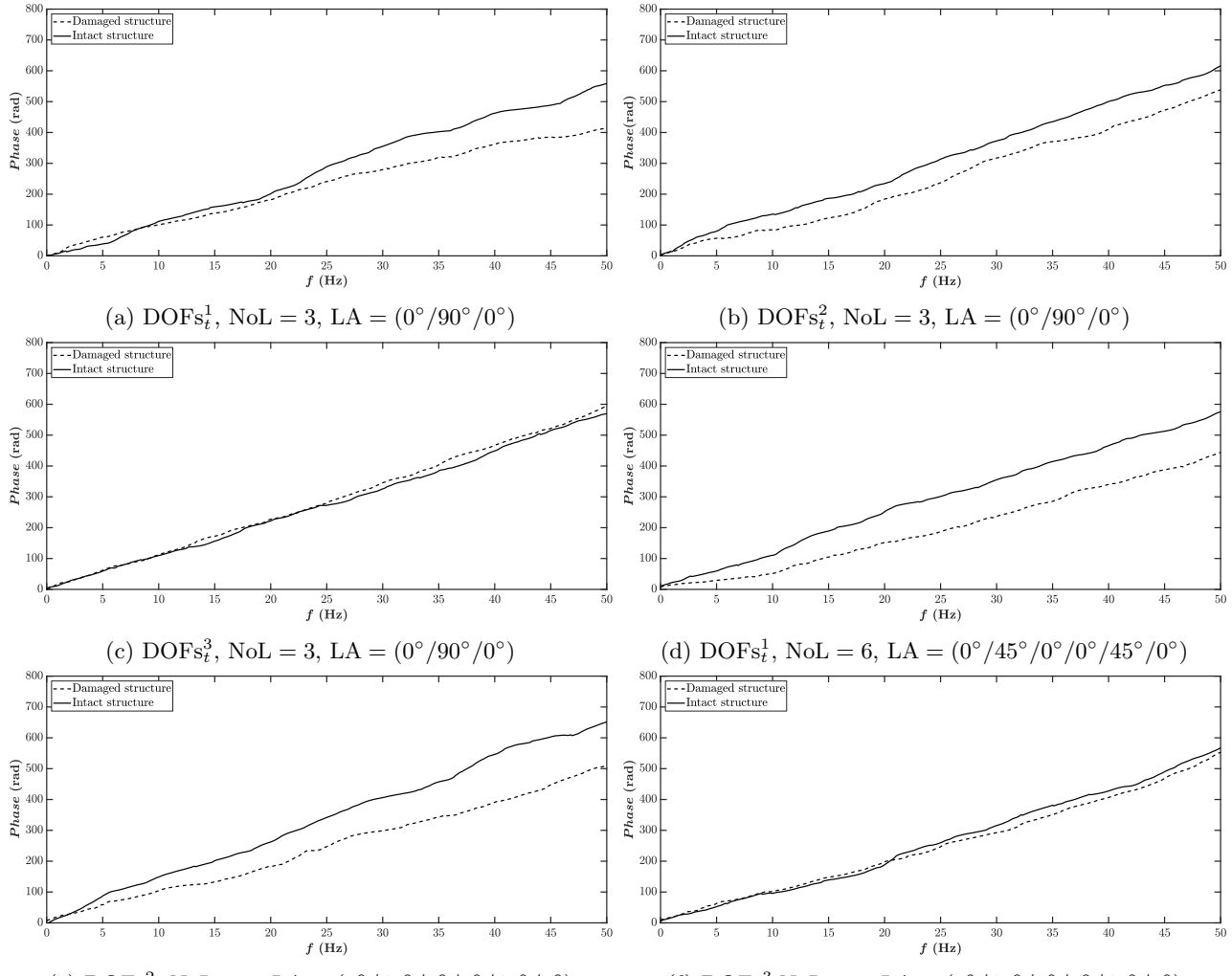

(a) DOFs$_t^1$, NoL = 3, LA = (0°/90°/0°)

(b) DOFs$_t^2$, NoL = 3, LA = (0°/90°/0°)

(c) DOFs$_t^3$, NoL = 3, LA = (0°/90°/0°)

(d) DOFs$_t^1$, NoL = 6, LA = (0°/45°/0°/0°/45°/0°)

(e) DOFs$_t^2$, NoL = 6, LA = (0°/45°/0°/0°/45°/0°)

(f) DOFs$_t^3$,NoL = 6, LA = (0°/45°/0°/0°/45°/0°)

Figure 8: The SUIHP of the damaged and healthy composite laminate for all studied models (scenario 4).

Table 6: The optimal excitation locations obtained for the laminated composite plate with different configurations. The DOFs corresponding to DOFs$_t^2$ are in bold font.

Plate	$\tilde{\Lambda}$	DOFs
NoL = 3, **LA** = (0°/90°/0°)	25.24, 23.65, 20.19, 17.25, 17.23, **17.05**, **16.25**	71, 66, 56, 31, 101, **47**, **72**
NoL = 6, **LA** = (0°/45°/0°/0°/45°/0°)	34.07, 33.74, 33.22, 32.08, **27.25**, **22.54**, **18.25**	21, 66, 31, 41, **107**, **117**, **122**

are presented here as an example, though the similar results were obtained for other damage scenarios.

The optimum excitation DOFs were selected based on the concept introduced in Section 4, i.e. using Eq.32. The maximum values of $\tilde{\Lambda}$ occurred at the first and second transitional DOFs. Table 6, shows the optimal excitation locations obtained for the two composite models.

It is evident from Figure 8 that the maximum variability of $\tilde{H}(f)$, due to damage, was achieved when the measurements were made from the first and second translational DOFs, i.e. DOFs$_t^1$ and DOFs$_t^2$, respectively. Therefore, more accurate results are expected to be obtained for damage indices, using $\tilde{H}(f)$ constructed based on measurements made on DOFs$_t^1$ and DOFs$_t^2$.

6.4. Damage detection using the proposed sensitivity method

The proposed sensitivity method solves the problem of damage detection in one stage. Therefore, the number of unknown damage indices is equal to the total number of the elements. Both of SUIHP and CFRF signals were used for damage detection in this section. The coefficient of variation (COV) was used in this paper to evaluate the performance of the algorithm when each of the CFRF and SUIHP was used for damage detection. The COV is defined as the normalized standard deviation of the vector of updated damage indices divided by its mean value [21, 18]. As such, a smaller value of the COV corresponds to a more robust prediction of the damage indices. Figs. 9 and 11 show the computed damage indices for the composite laminate structure with ply orientation (0°/90°/0°) when the SUIHP and CFRF matrices were contaminated with different amount of noise, i.e. NP=20 and NP=30, respectively. Here, the incomplete measurement ratio (IMR) indicates the ratio of the number of measured DOFs to the total number of DOFs. As such, the IMR=60% was assumed to be available for the laminated composite models. The damage indices were obtained after 50 runs to satisfy the convergence criteria, i.e. $|\delta\alpha_t| \leq 10^{-7}$. It is evident from the results that using SUIHP brings about far more accurate results than CFRF.

Figs. 10 and 12 show the obtained values of the COV for different models of the composite plate using the SUIHP and CFRF matrices with NP=30. It is evident from the results that using SUIHP is more reliable than the CFRF.

Table 7 presents the calculated accuracy indices for all models and damage scenarios. It is evident from the results that using SUIHP brings about much more accurate results than using CFRF.

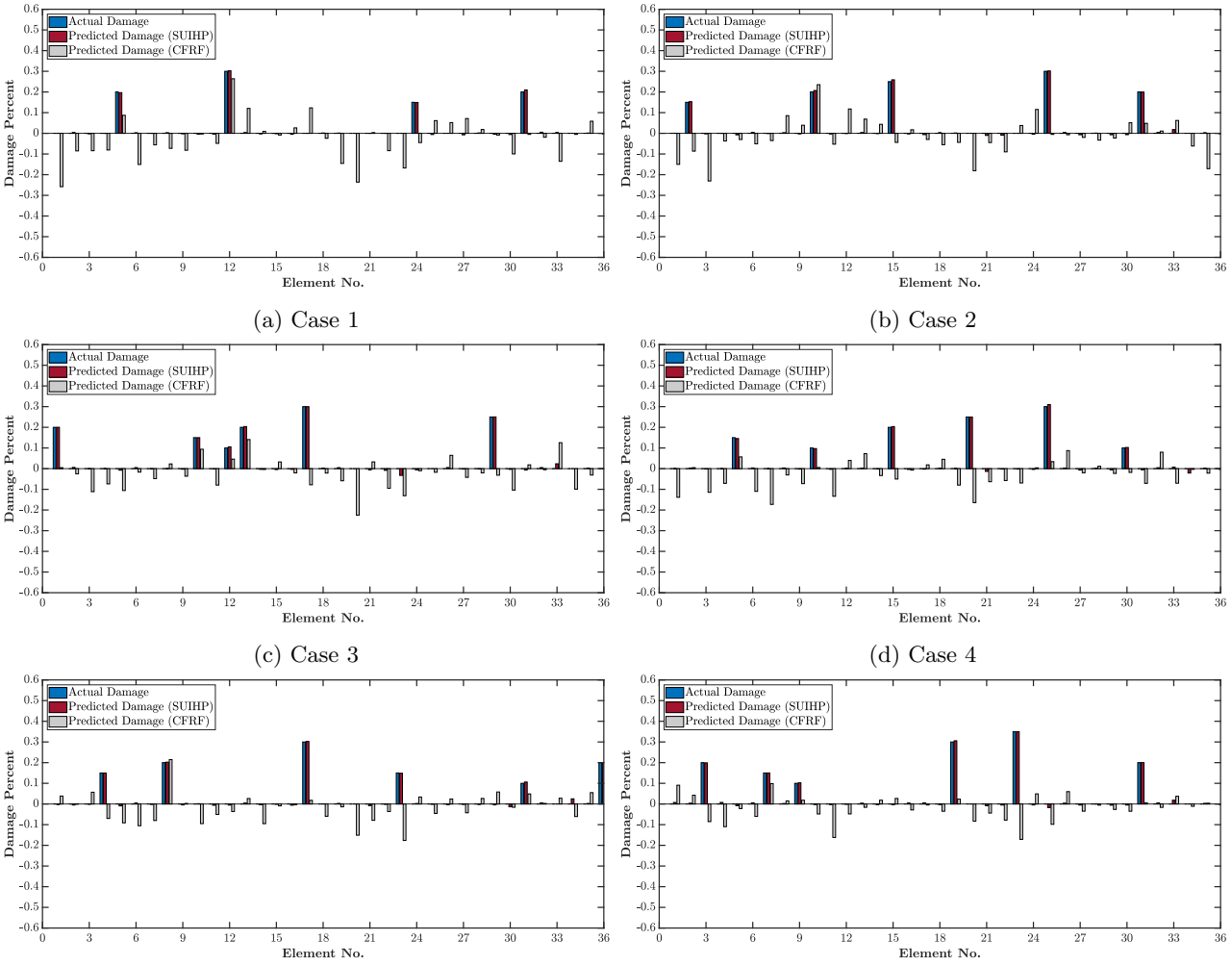

(a) Case 1

(b) Case 2

(c) Case 3

(d) Case 4

(e) Case 5

(f) Case 6

Figure 9: The predicted damage indices using CFRF and SUIHP in the proposed sensitivity-based model-updating method for damage scenarios 1-6 in the three-layer (0°/90°/0°) composite laminate plate (IMR = 60% and NP=30%)

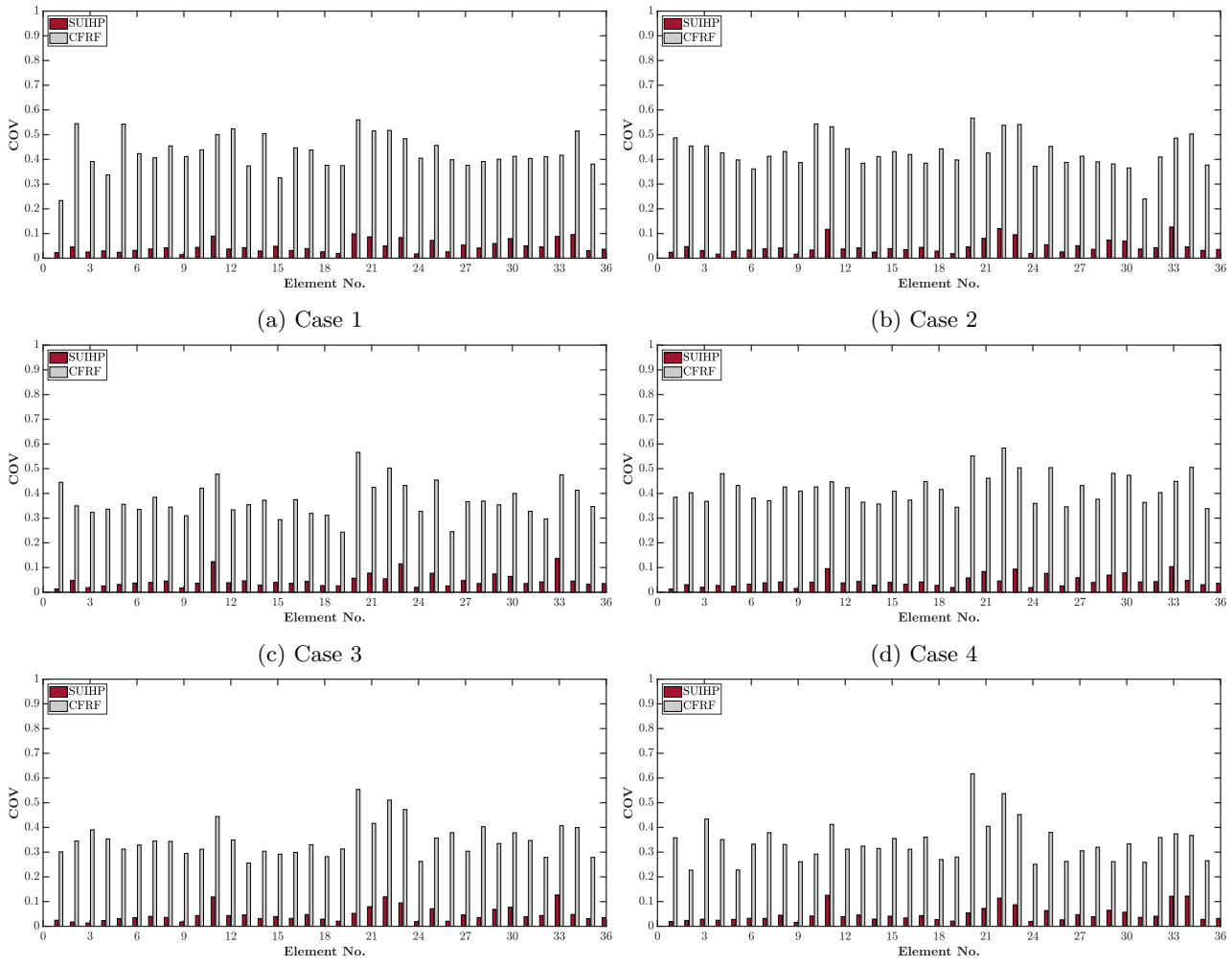

(a) Case 1

(b) Case 2

(c) Case 3

(d) Case 4

(e) Case 5

(f) Case 6

Figure 10: The COV indices using CFRF and SUIHP in the proposed sensitivity-based model-updating method for damage scenarios 1-6 in the three-layer (0°/90°/0°) composite laminate plate (IMR = 60% and NP=30%).

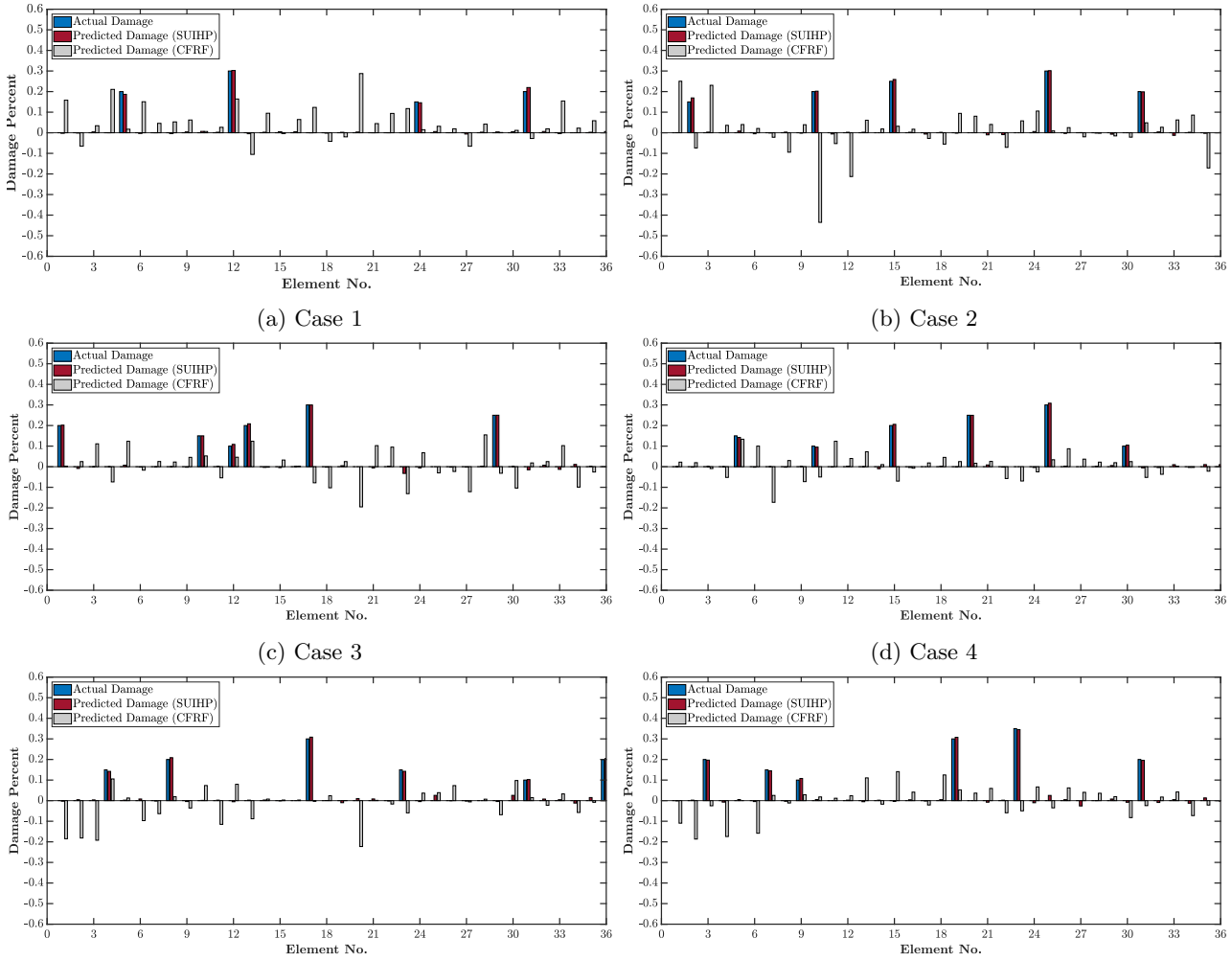

(a) Case 1

(b) Case 2

(c) Case 3

(d) Case 4

(e) Case 5

(f) Case 6

Figure 11: The predicted damage indices using CFRF and SUIHP in the proposed sensitivity-based model-updating method for damage scenarios 1-6 in the six-layer (0°/45°/0°/0°/45°/0°) composite laminate plate (IMR = 60% and NP=30%)

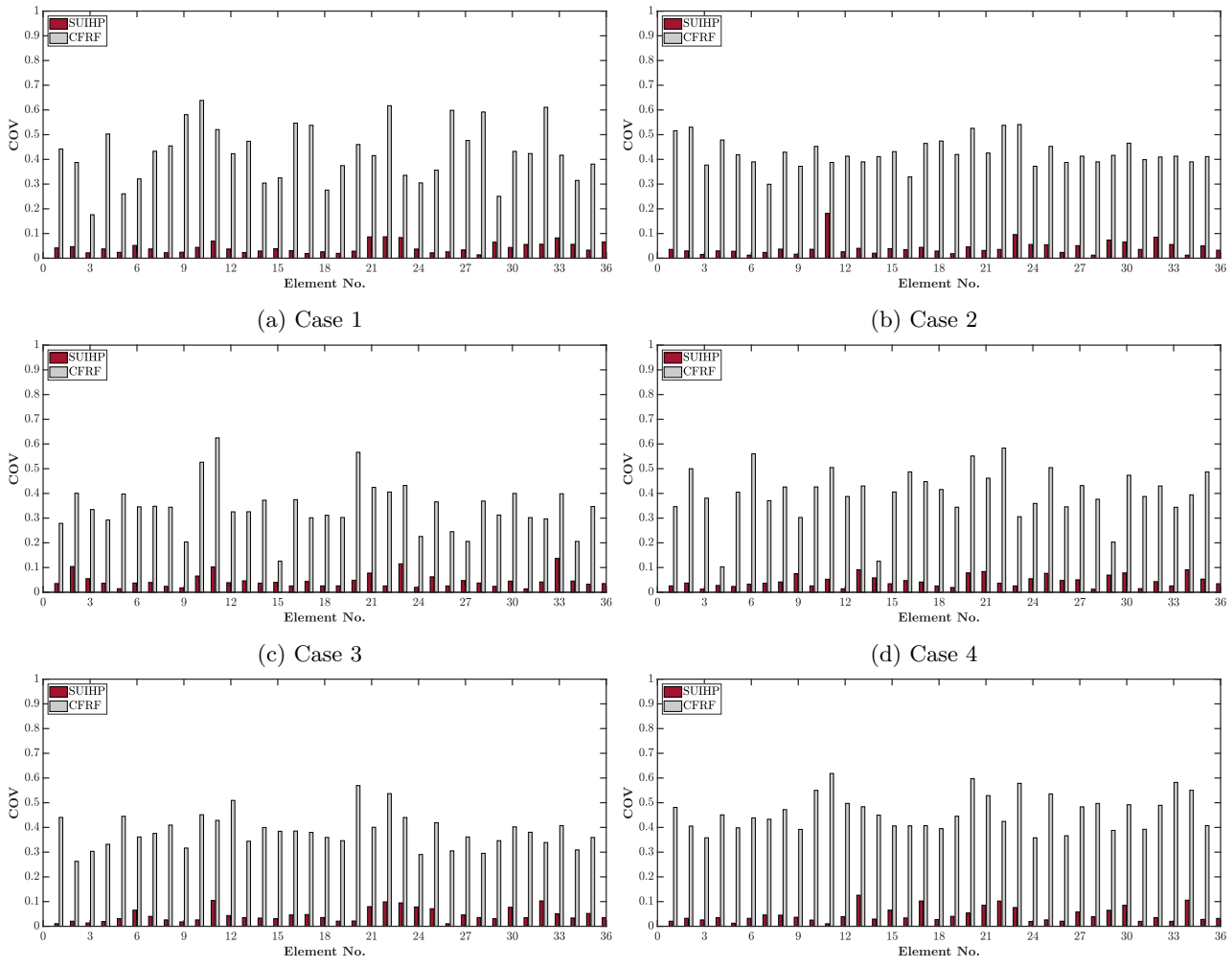

(a) Case 1

(b) Case 2

(c) Case 3

(d) Case 4

(e) Case 5

(f) Case 6

Figure 12: The COV indices using CFRF and SUIHP in the proposed sensitivity-based model-updating method for damage scenarios 1-6 in the six-layer (0°/90°/0°) composite laminate plate (IMR = 60% and NP=30%).

Table 7: Summary of the obtained error indices using the proposed sensitivity-based model-updating method for all damage cases in the studied composite laminate plates with different NPs; IMR=60%.

Case	Applied	NP	NoL = 3, LA = (0°/90°/0°)			NoL = 6, LA = (0°/45°/0°/0°/45°/0°)		
No.	method		MSE	RE	CI	MSE	RE	CI
1	SUIHP	20	0.0028	-0.1085	0.9588	0.0025	-0.0902	0.9628
1	CFRF	20	0.0474	-1.9690	0.3492	0.0304	-1.9377	0.3356
1	SUIHP	30	0.0038	-0.1196	0.9269	0.0026	-0.1003	0.9524
1	CFRF	30	0.0823	-1.9467	-0.4696	0.0822	-2.3095	-0.4583
2	SUIHP	20	0.0069	-0.2046	0.9242	0.0023	-0.1063	0.9279
2	CFRF	20	0.0320	-1.3615	0.3488	0.0290	-1.2695	0.3333
2	SUIHP	30	0.0071	-0.2831	0.8544	0.0040	-0.1308	0.9353
2	CFRF	30	0.0481	-1.5930	0.0067	0.0854	-1.2474	-0.3754
3	SUIHP	20	0.0027	-0.1038	0.9493	0.0085	-0.3041	0.8823
3	CFRF	20	0.0325	-0.9180	0.4760	0.0213	-0.9275	0.5123
3	SUIHP	30	0.0044	-0.1312	0.9101	0.0088	-0.3222	0.8500
3	CFRF	30	0.0770	-0.7856	-0.2929	0.0202	-1.563	0.1735
4	SUIHP	20	0.0034	-0.0903	0.9601	0.0034	-0.1001	0.9604
4	CFRF	20	0.0501	-1.6190	0.1288	0.0504	-1.6280	0.1797
4	SUIHP	30	0.0037	-0.0981	0.9394	0.0040	-0.1165	0.9307
4	CFRF	30	0.0643	-0.4848	-0.1775	0.0825	-0.8764	-0.4496
5	SUIHP	20	0.0061	-0.1452	0.9193	0.0031	-0.1236	0.9623
5	CFRF	20	0.0522	-1.7642	0.2266	0.0532	-1.8547	0.3362
5	SUIHP	30	0.0059	-0.1666	0.8931	0.0038	-0.1276	0.9236
5	CFRF	30	0.0774	-0.9460	-0.3663	0.0694	-0.7950	-0.2895
6	SUIHP	20	0.0162	-0.4024	0.8037	0.0042	-0.1128	0.9369
6	CFRF	20	0.0424	-1.4224	0.3118	0.0526	-1.8236	0.4256
6	SUIHP	30	0.0138	-0.4322	0.7735	0.0044	-0.1209	0.9371
6	CFRF	30	0.1188	-4.0888	-0.7550	0.0765	-0.3227	-0.3290

6.5. 120-element 3D truss model

Truss structures are another type of structures that can exhibit closely-spaced eigenvalues. Here, a 120-bar dome truss, first analyzed in [40] and further studied in [18, 41], is employed to further assess the capability of the proposed damage detection method. Figure 13 shows the sketch of the studied 120-bar dome truss. The mechanical and geometrical properties of the truss model are listed as follows:

- It comprises 120 bar elements with 49 nodes with three translational DOFs at each node.
- There are 111 active DOFs after imposing the boundary conditions at 12 hinged supports.
- The cross-section of all elements is equal to 0.01 m^2.
- The modulus of elasticity and density of the material are respectively 2×10^{11} $\frac{N}{m^2}$ and 7780 $\frac{kg}{m^3}$.

Table 8 lists the considered four damage scenarios for assessing the capability of the proposed method in damage detection of the truss structure. Subsequently, Table 9 presents the first 10 natural frequencies of the truss obtained for all the damage scenarios. The closely-spaced eigenvalues of the truss structure can be clearly seen from the table, in all the cases, where in some cases it appears that the modes are literally repeated. Note that here the obtained natural frequencies values are truncated to two decimal places. It is also evident from the table that the effect of damage appears as a decrease in the natural frequencies.

Table 8: Damage scenarios considered for the 120-member spatial truss (El. No.= Element number & S.R.= Stiffness reduction).

Case 1		Case 2		Case 3		Case 4	
El. No.	S.R.	El. No.	S.R.	El. No.	S.R.	El. No.	S.R.
1	0.15	9	0.10	21	0.20	42	0.35
10	0.20	19	0.25	31	0.10	54	0.20
28	0.30	35	0.30	54	0.30	69	0.25
70	0.20	89	0.30	62	0.25	76	0.20
		91	0.20	101	0.25	81	0.15
				117	0.20	100	0.35

Table 9: First ten natural frequencies of the 120-member spatial truss, in Hz.

Damage scenario	Mode No.									
	1	2	3	4	5	6	7	8	9	10
Intact	17.62	17.70	17.70	17.73	17.73	17.98	18.06	18.74	18.74	19.33
Case 1	17.18	17.64	17.64	17.69	17.73	17.92	18.01	18.60	18.73	19.16
Case 2	16.91	17.40	17.40	17.67	17.71	17.90	17.99	18.52	18.60	18.78
Case 3	17.38	17.48	17.48	17.62	17.69	17.89	17.99	18.58	18.64	18.97
Case 4	17.02	17.60	17.60	17.67	17.71	17.90	17.94	18.55	18.61	19.08

In this example, the structure is analysed with having two third of the active DOFs measured along the X and Y axes, i.e. IMR=67%. The optimum excitation locations were obtained at nine DOFs of 11, 26, 37, 61, 71, 86, 92, 101 and 107.

The FRD value of the first ten modes of the truss are listed in Table 10. Accordingly, the pairs of adjacent frequencies of these modes are either "close" or "very close", making the process of damage detection for this structure more complicated. Table 11 shows the computed accuracy indices for the results of the application of both of the SUIHP and CFRF to the damage detection problem of the truss structure. The results again demonstrate the far better performance of the SUIHP with respect to the CFRF in this case.

The predicted damage indices using SUIHP and CFRF are presented in Figs. 14, 15, 16, and 17. The obtained results clearly indicate the superiority of the application of SUIHP for damage detection at the presence of high percentage of noise. Moreover, the obtained values for COV also demonstrate the reliability of the results obtained from the SUIHP compared with the CFRF.

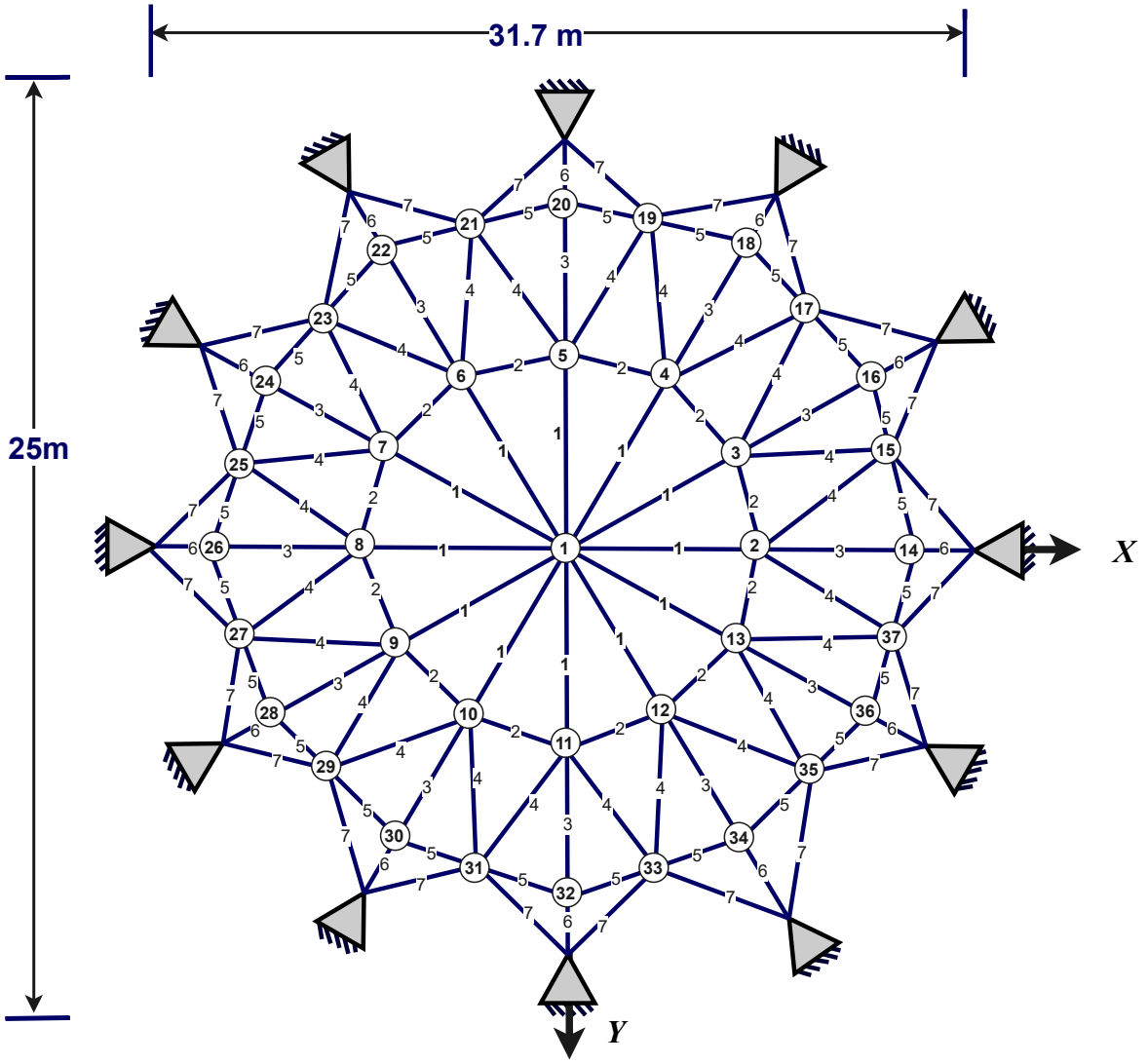

(a)

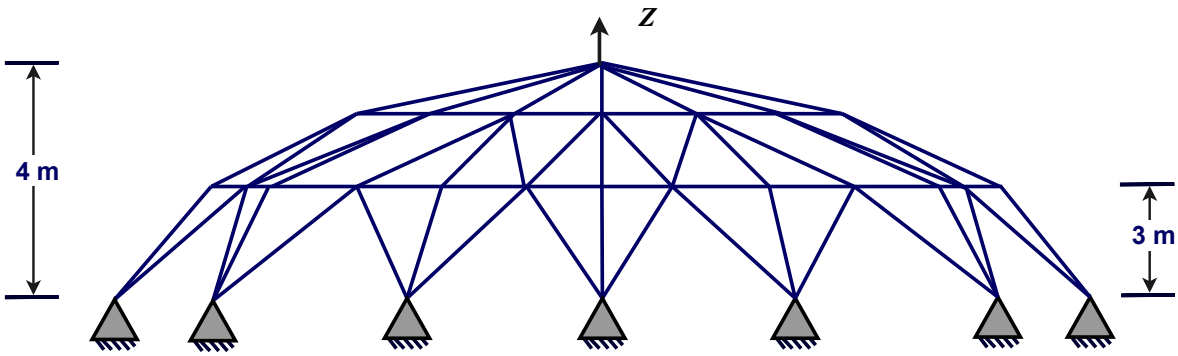

(b)

Figure 13: The 120-member spatial truss [18, 41].

Table 10: The $FRD_{i,j}$ values obtained for the first ten modes of the 120-member spatial truss.

Mode No.	$FRD_{i,j}$ (%)	Modal disparity
[1, 2]	0.5600	Very close
[2, 3]	1.95e-06	Very close
[3, 4]	1.7080	Close
[4, 5]	0.4391	Very close
[5, 6]	1.2415	Close
[6, 7]	1.3154	Close
[7, 8]	1.2507	Close
[8, 9]	5.85e-06	Very close
[9, 10]	4.7370	Close
[10, 11]	0.2926	Very close

Table 11: Summary of the obtained error indices using the proposed sensitivity-based model-updating method for all damage cases in the studied spatial truss model; IMR=67%.

Case No.	**Applied method**	**NP**	**MSE**	**RE**	**CI**
1	SUIHP	20	0.0028	-0.2085	0.9488
1	CFRF	20	0.0500	-4.9690	0.3482
1	SUIHP	30	0.0019	-0.2640	0.9106
1	CFRF	30	0.0507	-5.5210	-0.8816
2	SUIHP	20	0.0039	-0.2046	0.9442
2	CFRF	20	0.0420	-3.3615	0.4488
2	SUIHP	30	0.0022	-0.2236	0.9233
2	CFRF	30	0.0576	-4.2427	-0.6534
3	SUIHP	20	0.0025	-0.1238	0.9483
3	CFRF	20	0.0425	-2.9180	0.4860
3	SUIHP	30	0.0020	-0.1597	0.9285
3	CFRF	30	0.0594	-3.5629	-0.6845
4	SUIHP	20	0.0034	-0.0903	0.9601
4	CFRF	20	0.0501	-2.6190	0.4289
4	SUIHP	30	0.0020	-0.1499	0.9413
4	CFRF	30	0.0693	-3.7756	-0.7296

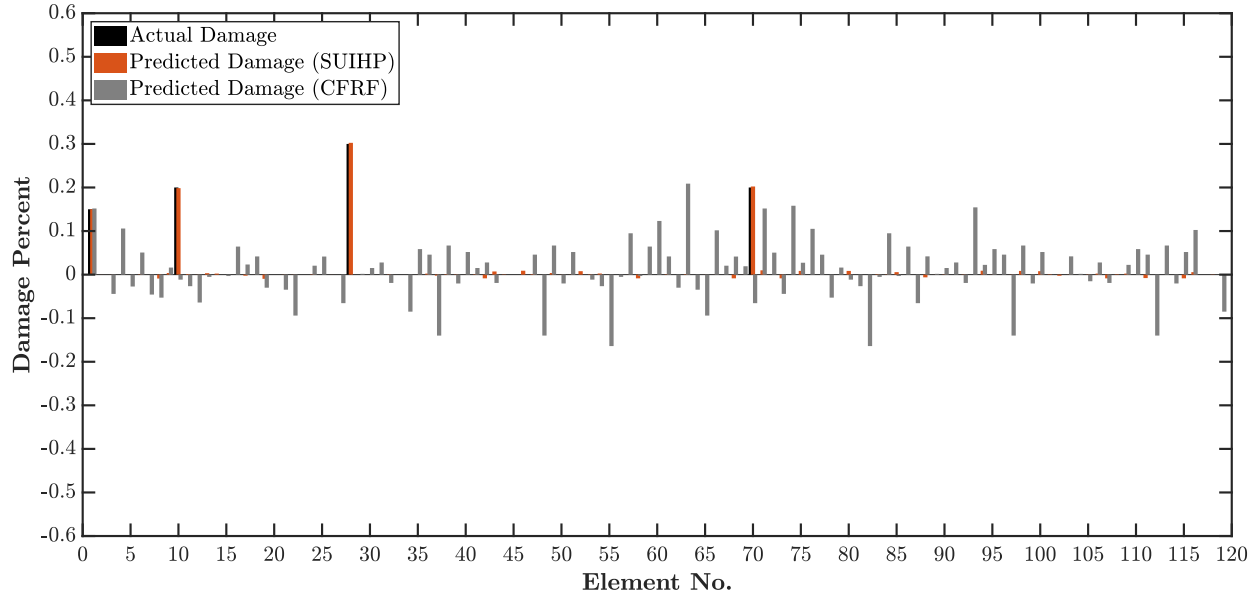

(a)

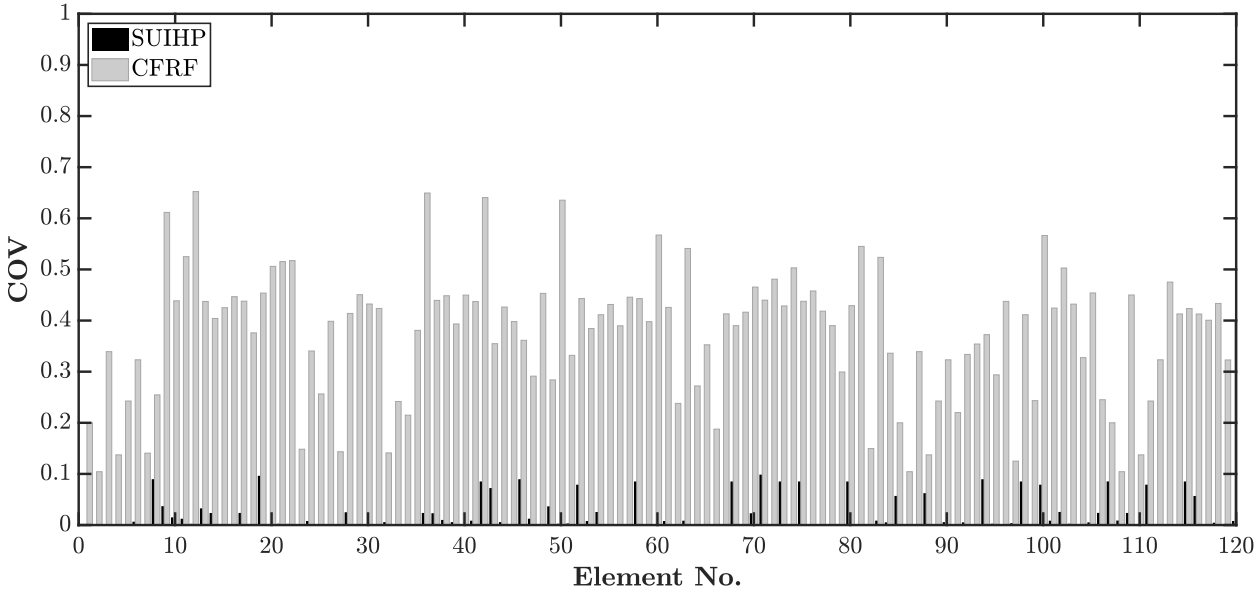

(b)

Figure 14: (a) The predicted damage parameters for the damage scenario 1 of the 3D truss elements, and (b) the COV values of the predicted parameters; IMR=67%, NP=30.

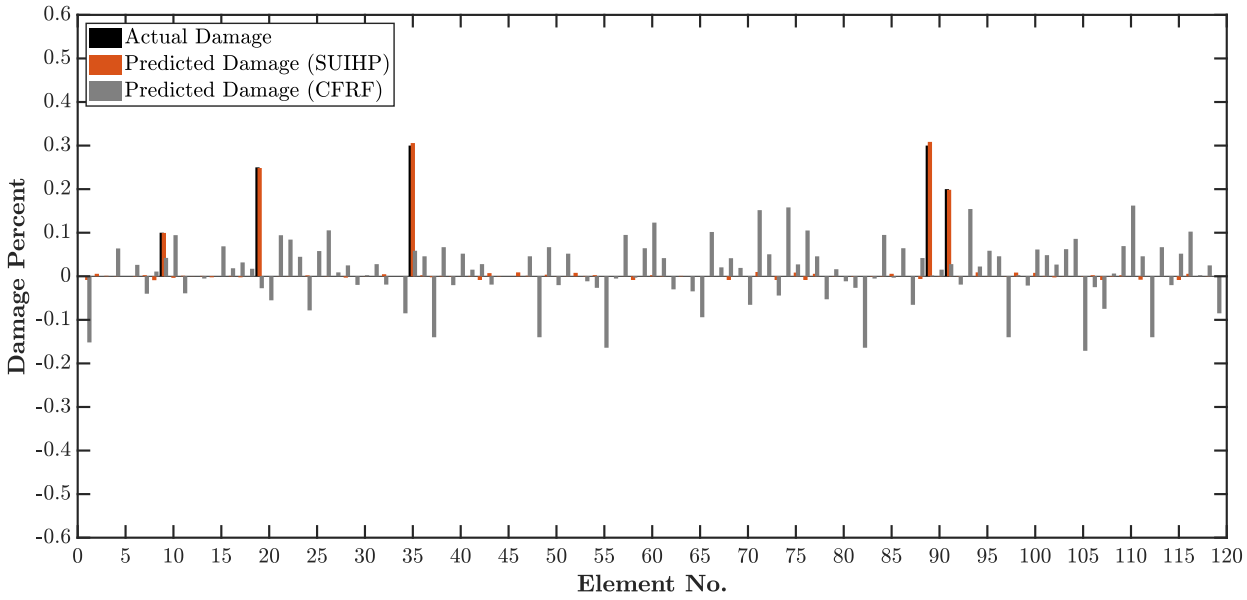

(a)

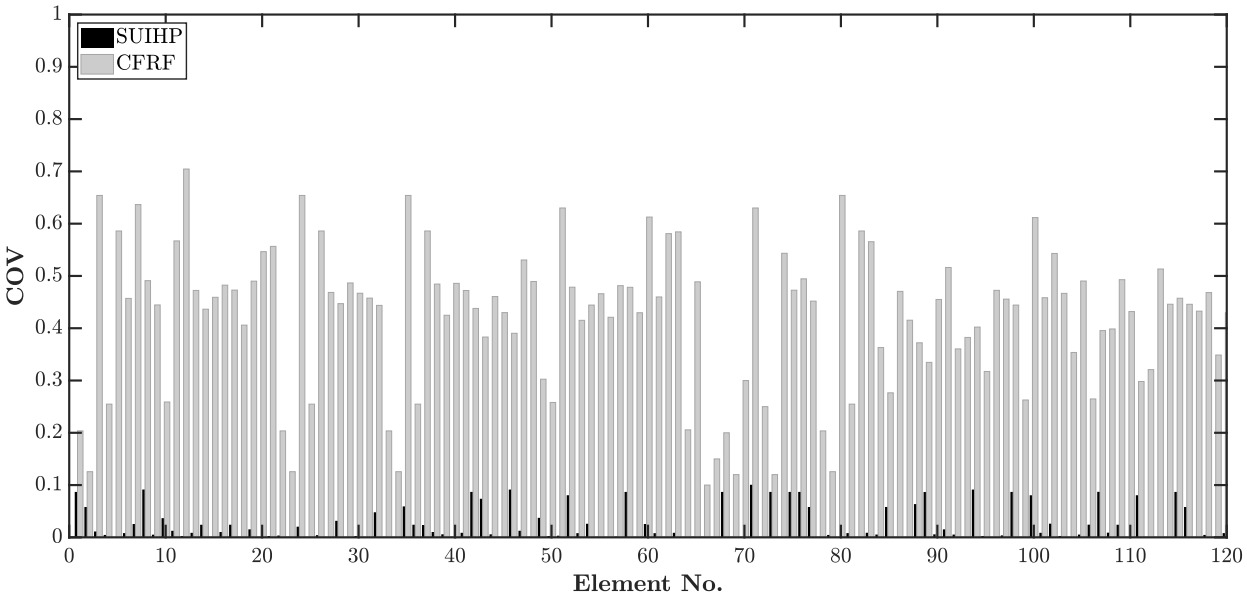

(b)

Figure 15: (a) The predicted damage parameters for the damage scenario 2 of the 3D truss elements, and (b) the COV values of the predicted parameters; IMR=67%, NP=30.

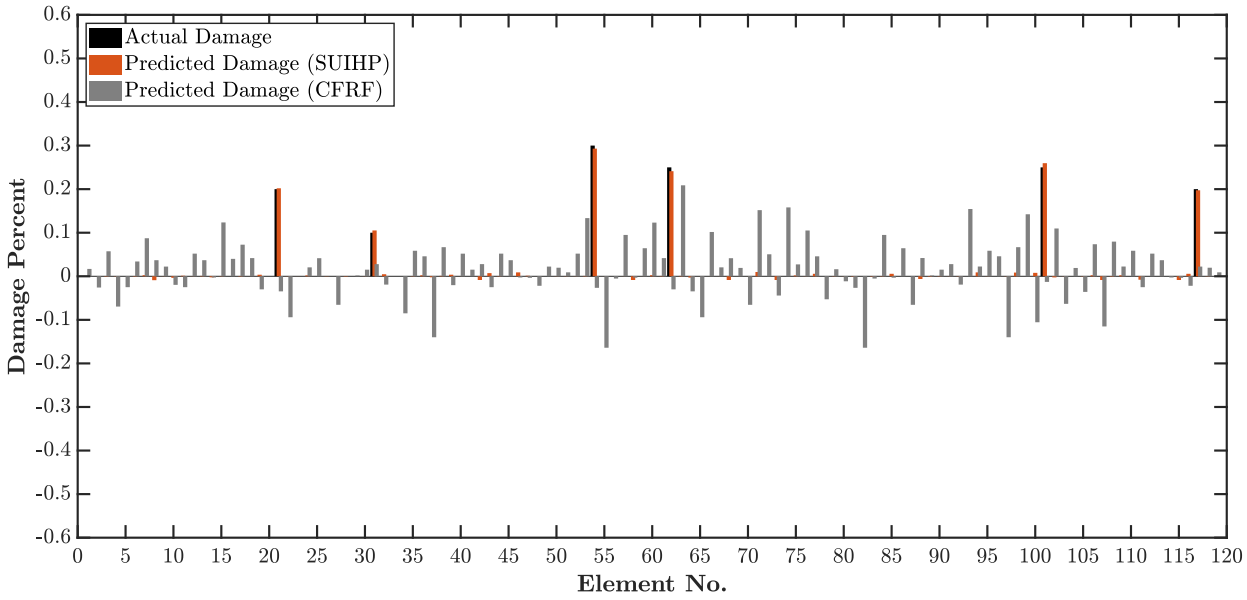

(a)

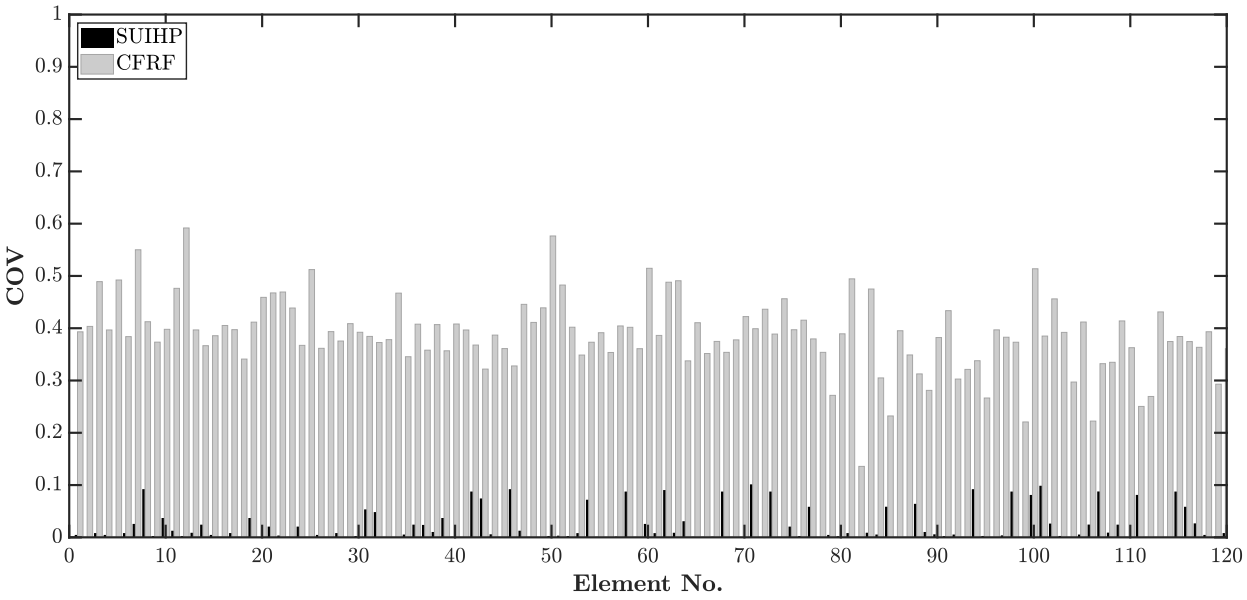

(b)

Figure 16: (a) The predicted damage parameters for the damage scenario 3 of the 3D truss elements, and (b) the COV values of the predicted parameters; IMR=67%, NP=30.

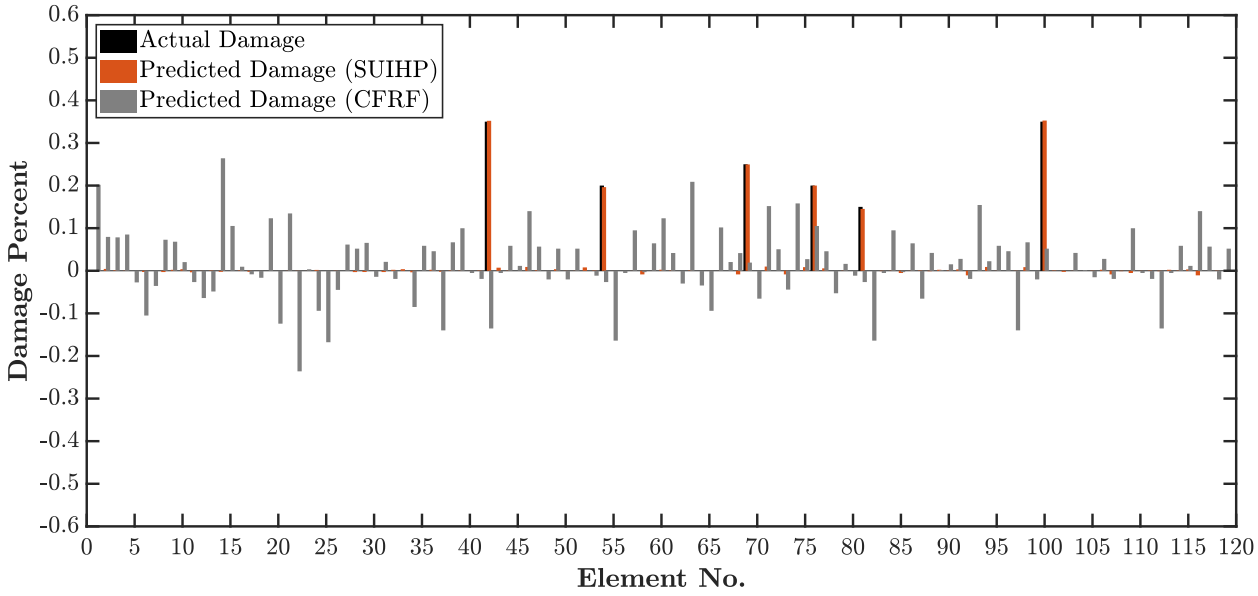

(a)

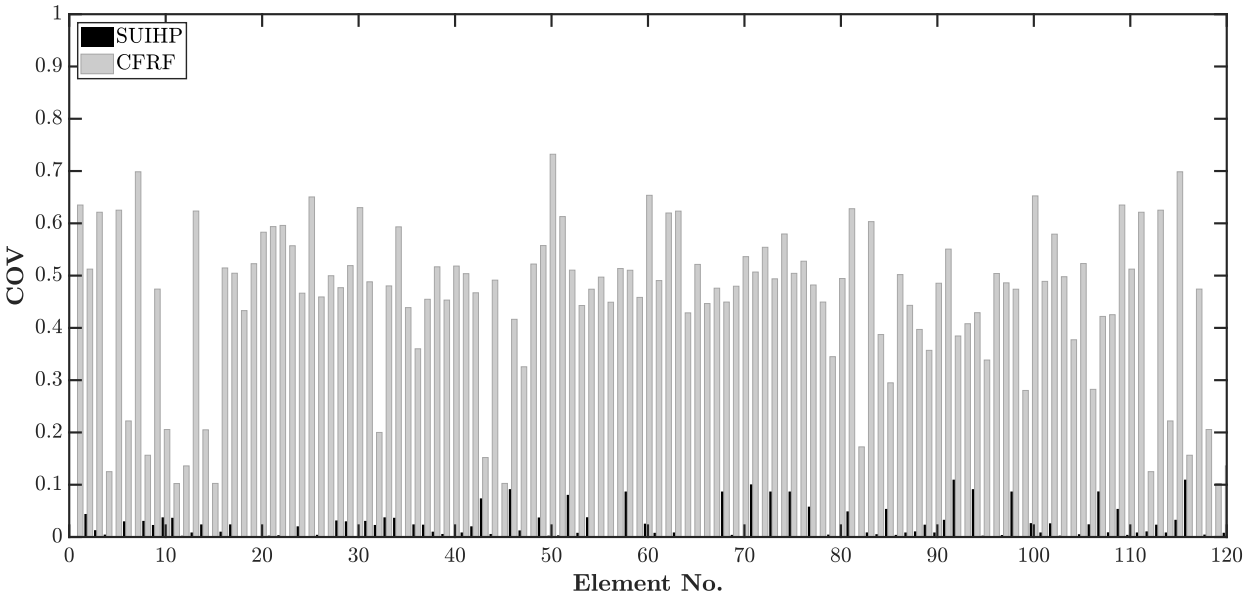

(b)

Figure 17: (a) The predicted damage parameters for the damage scenario 4 of the 3D truss elements, and (b) the COV values of the predicted parameters; IMR=67%, NP=30.

7. Significance of extracting residual IMF

Thus far, the SUIHP obtained through discarding the first and residual IMFs extracted from decomposing a CFRF using EMD was used for damage detection. It is generally meaningful to discard the IMF with the highest center frequency (first IMF), as it usually corresponds to noise in a signal. However, the significance of discarding the residual IMF is not obvious. This prompt the study of damage detection results obtained from using the SUIHP with and without discarding the residual IMF. In this section, the notations $\text{SUIHP}_{\text{full}}$ and $\text{SUIHP}_{\text{dis}}$ represent the SUIHP with and without the residual IMF, respectively.

Note that a general decision cannot be made based on the results obtained from one-time running of the damage detection algorithm. Therefore, in order to investigate the effectiveness of discarding the residual IMF, the COV obtained through running of the damage detection algorithm on CFRFs contaminated with 50 different noises is presented in this section for both the plate and truss structures. The third damage scenario of each case is considered as an example, though similar results were obtained for other damage scenarios. Figure 18 depicts the obtained results for different structures. Accordingly, it is obvious that discarding the residual IMF is more effective in the damage detection of the plate models. Regarding the truss structure, different results can be achieved for different elements. However, the difference is marginal and can be neglected. Further investigation of this issue in different structures can be the subject of a future work.

8. Convergence of the proposed algorithm

There are different ways to assess the convergence capability of a model updating algorithm. The convergence trace plot of an algorithm is a valid tool to check the power of the algorithm against overshooting. In this section, the trace plot of running the proposed algorithm on three different models is presented for damaged elements in one of the damage scenarios in each structure. Figure 19 shows the trace plots of the convergence of the algorithm for the calculation of the damage indices. The Figure shows that, in all cases, the algorithm converges to the exact solution after 15 runs. It can be also seen that no overshooting of the results occurs and the convergence curve is smoothly heading towards the exact solution. This indeed confirms the strong capability of the proposed method for damage detection in different types of structures.

9. Comparison with other methods

The proposed method of this paper is compared against two other methods from the literature, in terms of accuracy and the number of measure DOFs required for accurate damage detection. To this end,

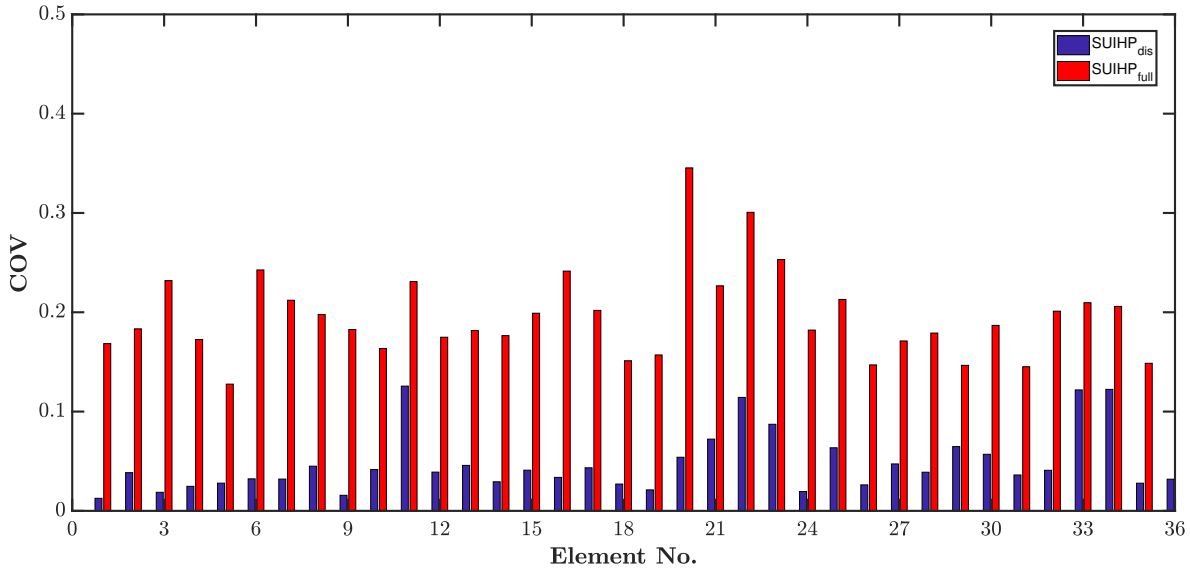

(a) Three-layer plate, NoL=(0°/90°/0°)

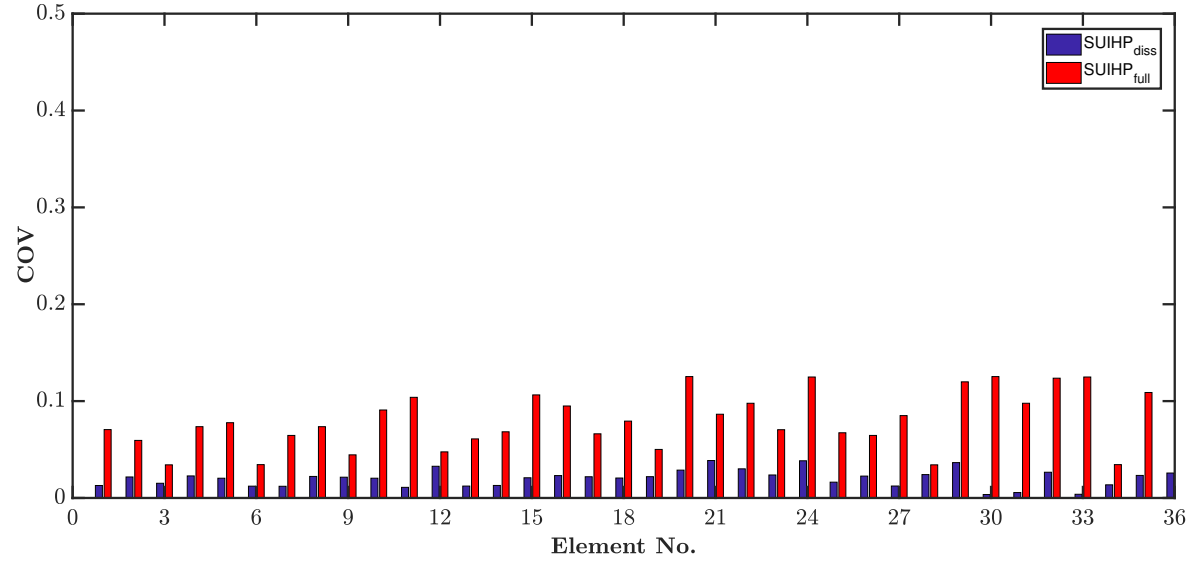

(b) Six-layer plate, NoL=(0°/45°/0°/0°/45°/0°)

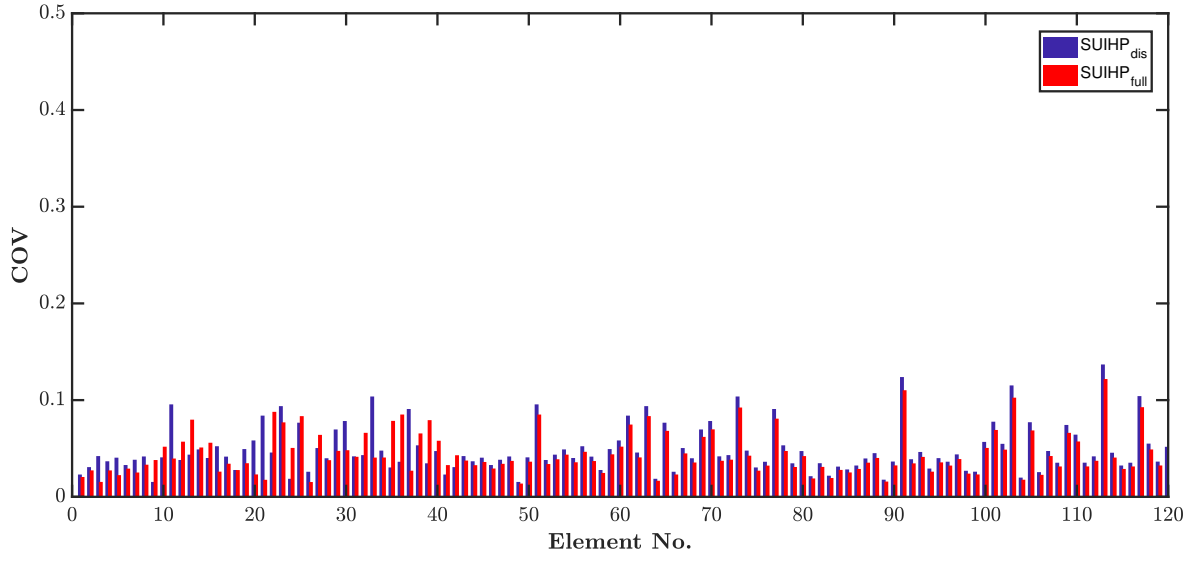

(c) Truss

Figure 18: The sensitivity of the proposed SUIHP to discarding the residual IMF when employed for damage detection of different structures.

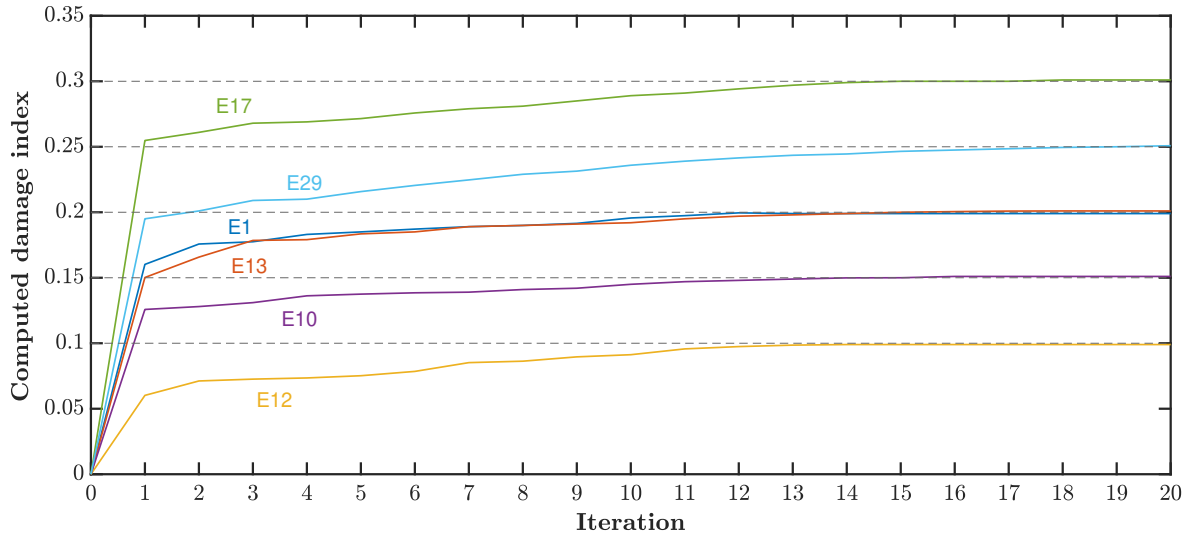

(a) Plate with NOL = 3, case 3

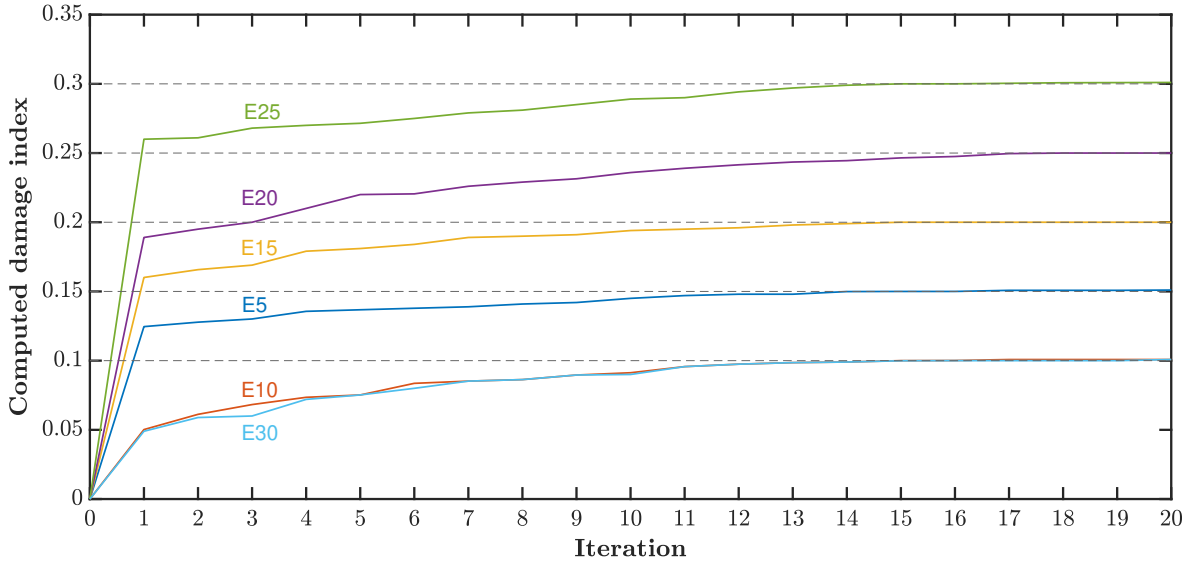

(b) Plate with NOL = 6, case 4

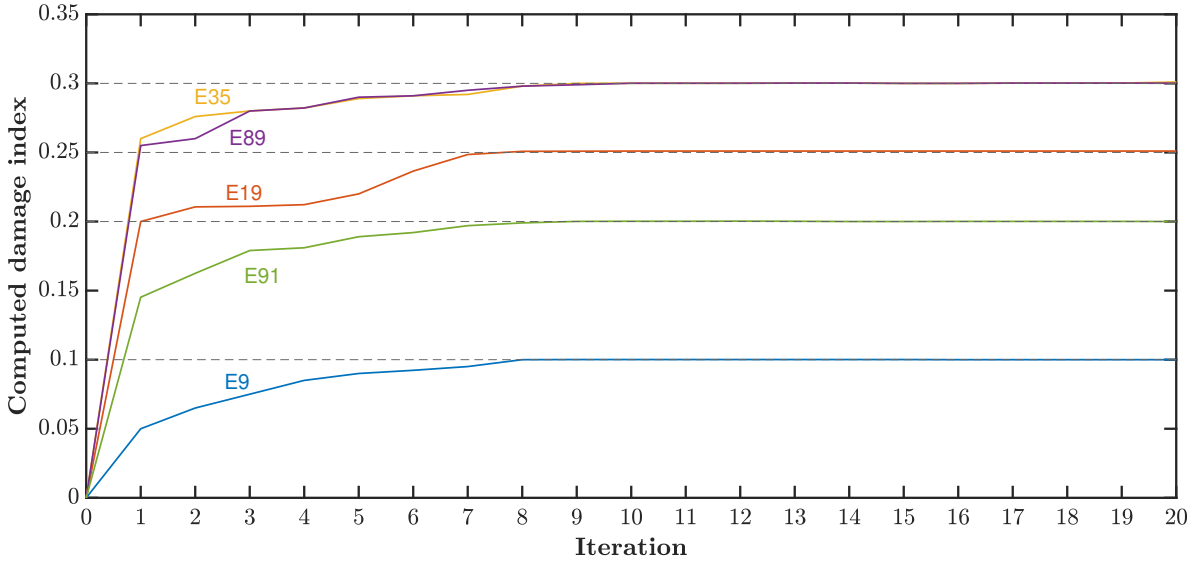

(c) Truss, case 2

Figure 19: The trace plot of running the proposed model updating algorithm on different models with different damaged elements in the specified damage scenarios.

only damage scenarios 3 and 4 in both examples of the composite and truss structures were considered to be solved using all the methods.

In [20] the finite element model of a structure is updated using an FRF-based model updating algorithm. The proposed model updating equation employs the harmonic forced vibration of the damaged structure, where changes induced in the FRF of the structure by damage are correlated with changes of the structural stiffness due to damage. The FRF of the intact structure and measured natural frequencies are exploited to construct the proposed damage sensitivity equations. Likewise, [21] employs updated structural stiffness parameters for damage detection, where changes in FRF due to damage are correlated with structural parameters (i.e. unknown damage indices). The proposed method, however, is a sensitivity-based model updating algorithm. It also favors a plain approximation to alleviate the negative effects of unmeasured FRFs. As such, the unmeasured FRFs of damaged structure are approximated through shifting the FRF data obtained from the FE model of the intact structure. The readers are referred to the original papers for further details.

Tables 12 and 13 show the accuracy indices obtained for the results of the application of the proposed method and the methods proposed in [20] and [21] to the composite and truss structures, respectively. The obtained values of the accuracy indicators MSE, RE, and CI clearly demonstrate the superiority of the proposed method in this paper. According to [20], the proposed method requires a few frequency points for model updating when the FRF data is contaminated with a low level of noise. However, as the level of noise increases more data with a higher sensitivity to the changes in parameters are required to guarantee a robust parameters estimation. This is a possible reason for the method in [20] to perform poorly when data with a high level of noise is available. Moreover, the capability of the method was examined through a 2D truss model, and therefore, its capability in damage detection of more complex structures was not validated. Regarding the method proposed in [21], the FRF data of a 2D truss example was contaminated with 15% noise. However, the method was not applied to a more complex form of structure with higher level of noise. Therefore, its capability in damage detection of more complex structures, like the laminated composite model and the 3D truss model of this study, was not validated.

Figures 20 and 21 show the results of damage detection for the studied damage scenarios. The results clearly indicate the poor performance of the two other methods when applied to the structures under study. This also makes the presentation of the COV values obtained for these cases irrelevant, as they are fairly inaccurate. Therefore, the superiority of the proposed method of this paper can be concluded.

Table 12: Comparison of the accuracy indicators obtained for [20] and [21] with the proposed method when applied to the laminated composite plates; IMR=60%.

Case	**Applied**	**NP**	**NoL = 3, LA = (0°/90°/0°)**			**NoL = 6, LA = (0°/45°/0°/0°/45°/0°)**		
No.	**method**	**(%)**	**MSE**	**RE**	**CI**	**MSE**	**RE**	**CI**
3	Proposed	30	0.0044	-0.1312	0.9101	0.0088	-0.3222	0.8500
3	Proposed	40	0.0078	-0.2672	0.8640	0.0098	-0.4782	0.7200
4	Proposed	30	0.0037	-0.0981	0.9394	0.0040	-0.1165	0.9307
4	Proposed	40	0.0096	-0.3722	0.6505	0.0111	-0.3888	0.6239
3	[20]	30	0.1738	-0.6888	3.1256	0.2105	-0.7058	4.2256
3	[20]	40	0.3540	-0.8963	4.1026	0.3105	-0.6235	5.5656
4	[20]	30	0.1809	-0.8923	5.2369	0.2700	-0.9023	4.0028
4	[20]	40	0.4456	-0.8712	3.9999	0.2987	-0.6023	4.9999
3	[21]	30	0.2708	-0.8712	5.0012	0.3525	-0.8208	5.2366
3	[21]	40	0.4526	-0.9063	7.1026	0.6135	-0.8535	8.2356
4	[21]	30	0.2500	-0.8937	4.8963	0.2987	-0.7236	3.2639
4	[21]	40	0.3905	-0.9563	8.2365	0.5986	-0.8632	7.2354

Table 13: Comparison of the accuracy indicators obtained for [20] and [21] with the proposed method when applied to the truss structure; IMR=67%.

Case No.	**Applied method**	**NP (%)**	**MSE**	**RE**	**CI**
3	Proposed	30	0.0020	-0.1597	0.9285
3	Proposed	40	0.0045	-0.2072	0.8740
4	Proposed	30	0.0020	-0.1499	0.9413
4	Proposed	40	0.0038	-0.2222	0.8852
3	[20]	30	0.1838	-0.6568	3.0551
3	[20]	40	0.3341	-0.8093	3.1002
4	[20]	30	0.1990	-0.8902	5.2025
4	[20]	40	0.4266	-0.8072	3.9129
3	[21]	30	0.2638	-0.8651	5.3012
3	[21]	40	0.4528	-0.9123	7.2146
4	[21]	30	0.2502	-0.8837	4.2543
4	[21]	40	0.3965	-0.9023	8.1455

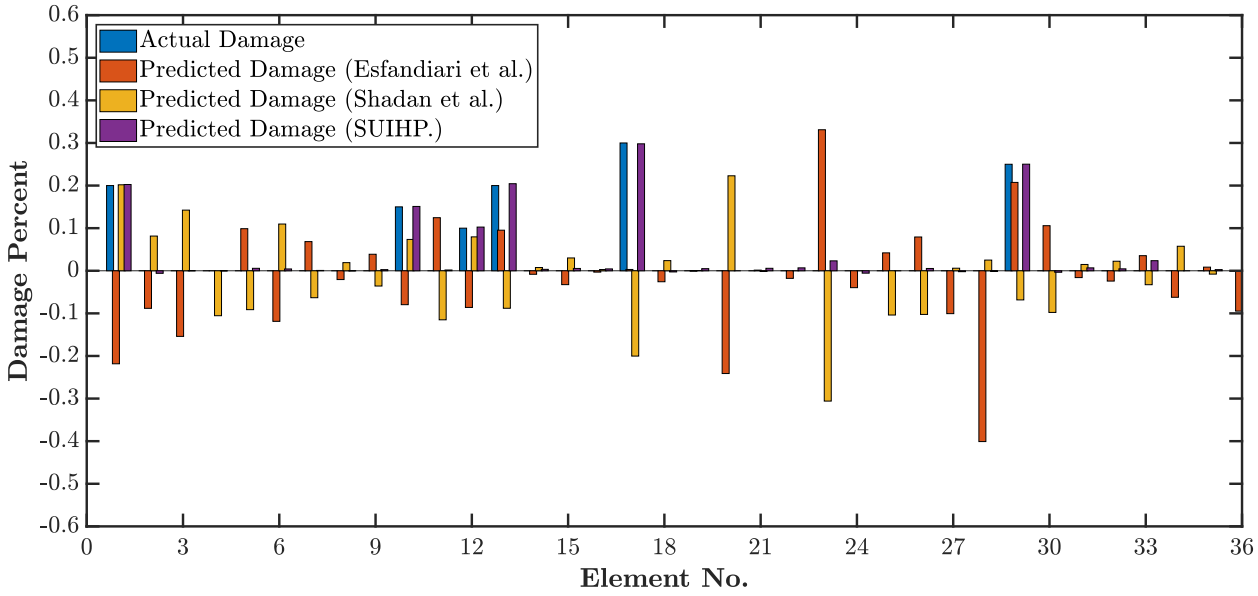

(a) Case 3

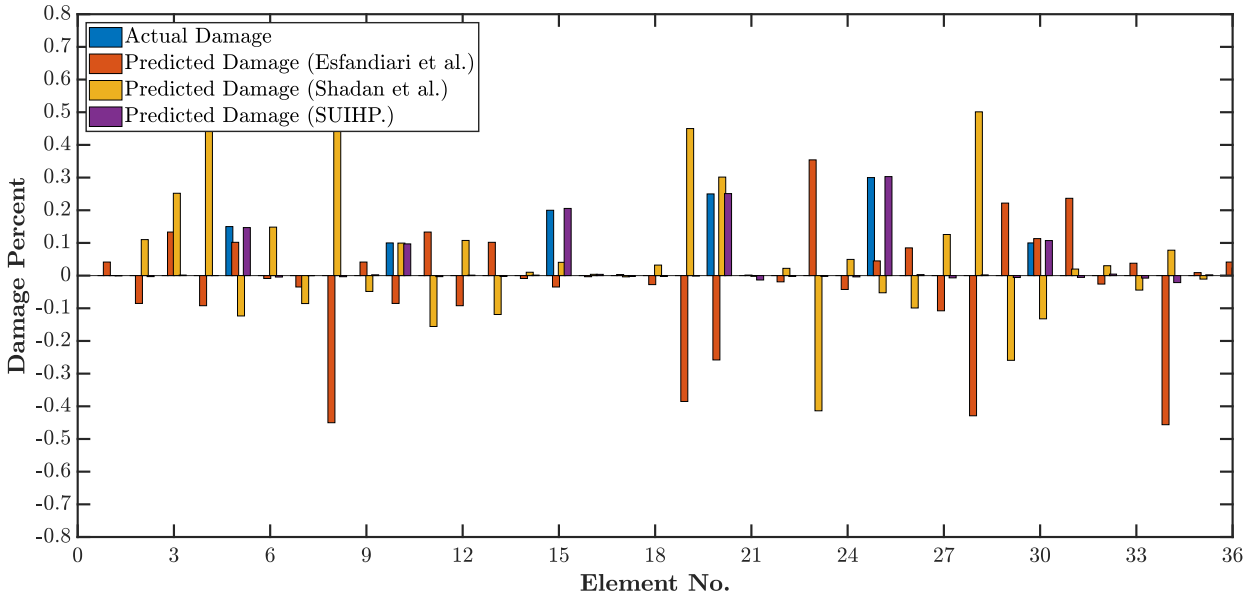

(b) Case 4

Figure 20: Comparison of the predicted damage indices for [20] and [21] with the proposed method when applied to the laminated composite structures; IMR=60%, NP=30.

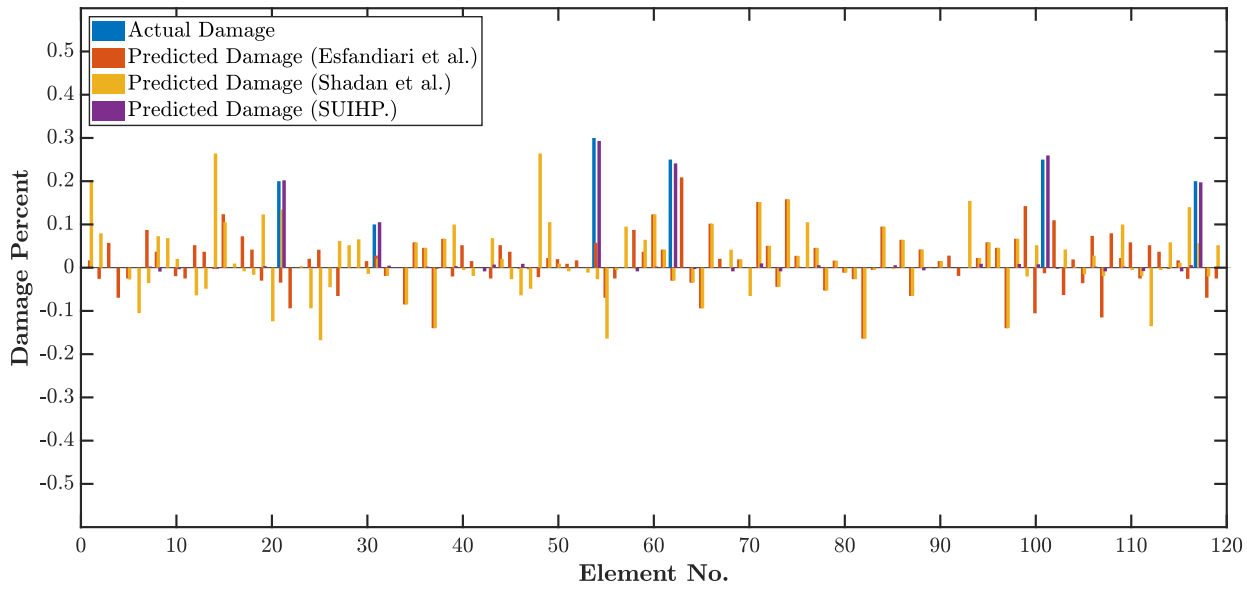

(a) Case 3

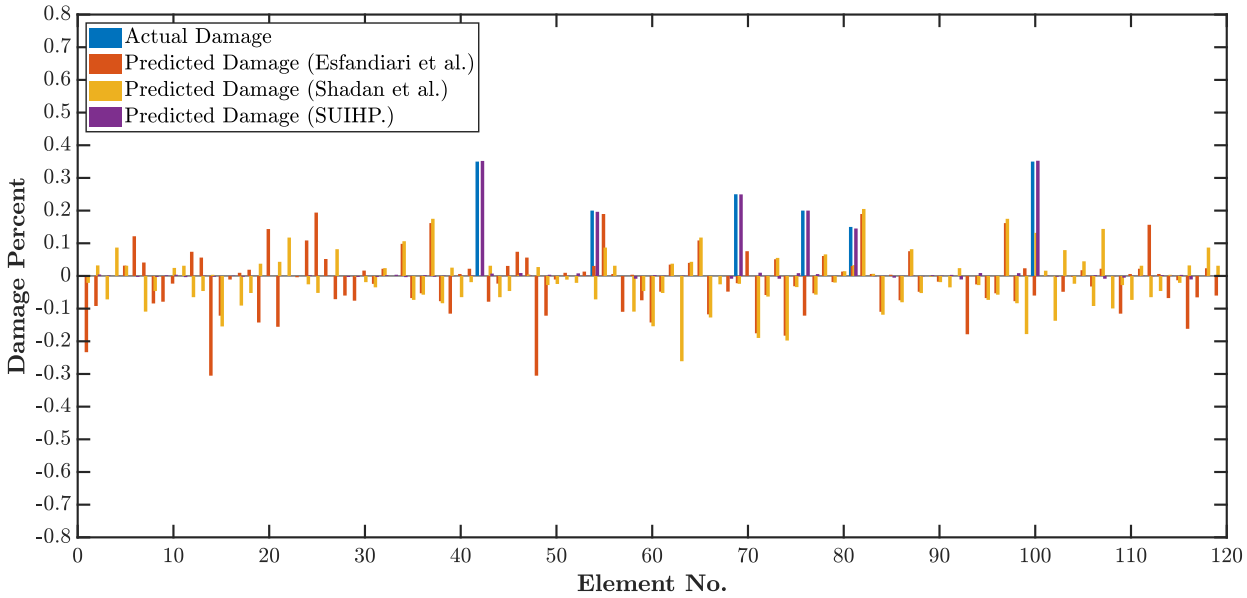

(b) Case 4

Figure 21: Comparison of the predicted damage indices for [20] and [21] with the proposed method when applied to the truss structure; IMR=67%, NP=30 .

10. Conclusions

In this study, a sensitivity-based model-updating damage detection method was proposed. The proposed method uses the SUIHP of the CFRF signals as input in the obtained equation for damage detection. The proposed SUIHP is constructed based on the summation of instantaneous Hilbert phase of the decomposed IMFs of a CFRF through EMD. Accordingly, the IMFs with the highest centre frequency and the residual IMF were discarded. While discarding the IMF with the highest centre frequency is meaningful as noise, the sensitivity of the effectiveness of the proposed DSF to discarding the residual IMF was further investigated. It was shown that the effect of removing the residual IMF on the results of damage detection in plate models is quite sensible. This effect, however, was not as much sensible for the truss structure, prompting further investigation of this issue in a future work. All in all, it was shown that the proposed method produces more accurate results at the presence of high percentage of noise. The proposed method was also compared against two other methods proposed in the literature and its superiority was demonstrated.

This paper presents several novelties other than the proposed damage detection method, such as proposing a method for finding optimal excitation locations for obtaining CFRF. While the results of this paper are promising, the authors are completely aware of possible limitations of a numerical study. For instance, the numerical models of the laminated composite structures studied in this paper are considered to follow the assumption of fully clamped boundary conditions. However, such an assumption may not be realistic when it comes to modeling a real composite structure. Therefore, care must be taken when an FE model of a real structure is used in any model updating problem, including the one proposed in this paper. Moreover, the present study is aimed at proposing a novel concept through coupling a nonlinear/nonstationary signal decomposition algorithm, i.e. EMD, with the classical concept of FRFs to deal with the challenging problem of damage detection in structures with closely-spaced eigenvalues. Therefore, the authors are well aware of the limitation of numerical studies and are on track to perform further experimental studies to validate the results of this study in their future work. As such, the current study is a concept paper that aims to conduct a parametric study of the developed model updating algorithm. Further experimental studies can serve as the second stage of this study that can further validate the applicability of the proposed method in real structures.

References

[1] Moughty JJ, Casas JR. A state of the art review of modal-based damage detection in bridges: Development, challenges, and solutions. Applied Sciences 2017;7(5):510. doi:10.3390/app7050510.

[2] Hassani S, Mousavi M, Gandomi AH. Structural health monitoring in composite structures: A comprehensive review. Sensors 2022;22(1):153. doi:10.3390/s22010153.

[3] Mousavi M, Holloway D, Olivier J, Gandomi AH. Beam damage detection using synchronisation of peaks in instantaneous frequency and amplitude of vibration data. Measurement 2021;168:108297.

[4] Hou R, Xia Y. Review on the new development of vibration-based damage identification for civil engineering structures: 2010–2019. Journal of Sound and Vibration 2020;:115741doi:10.1016/j.jsv.2020.115741.

[5] Friswell M, Penny J. Updating model parameters from frequency domain data via reduced order models. Mechanical Systems and Signal Processing 1990;4(5):377–91. doi:10.1016/0888-3270(90)90064-R.

[6] Friswell M, Mottershead JE. Finite element model updating in structural dynamics; vol. 38. Springer Science & Business Media; 2013.

[7] Barman SK, Maiti DK, Maity D. Vibration-based delamination detection in composite structures employing mixed unified particle swarm optimization. AIAA Journal 2021;59(1):386–99. doi:10.2514/1.J059176.

[8] Güemes A, Fernandez-Lopez A, Pozo AR, Sierra-Pérez J. Structural health monitoring for advanced composite structures: a review. Journal of Composites Science 2020;4(1):13. doi:10.3390/jcs4010013.

[9] Chen S, Ong ZC, Lam WH, Lim KS, Lai KW. Operational damage identification scheme utilizing de-noised frequency response functions and artificial neural network. Journal of Nondestructive Evaluation 2020;39(3):1–9. doi:doi.org/10.1007/s10921-020-00709-x.

[10] Feng D, Feng MQ. Computer vision for shm of civil infrastructure: From dynamic response measurement to damage detection–a review. Engineering Structures 2018;156:105–17. doi:10.1016/j.engstruct.2017.11.018.

[11] Liu X, Hu J. On the placement of actuators and sensors for flexible structures with closely spaced modes. Science China Technological Sciences 2010;53(7):1973–82. doi:10.1007/s11431-010-4028-y.

[12] Arora V, Singh S, Kundra T. Damped model updating using complex updating parameters. Journal of Sound and Vibration 2009;320(1-2):438–51. doi:10.1016/j.jsv.2008.08.014.

[13] Ganguli R. Wavelet based damage detection. In: Structural health monitoring. Springer; 2020, p. 161–92.

[14] Ma Q, Solís M, Galvín P. Wavelet analysis of static deflections for multiple damage identification in beams. Mechanical Systems and Signal Processing 2021;147:107103. doi:10.1016/j.ymssp.2020.107103.

[15] Mousavi M, Taskhiri MS, Holloway D, Olivier J, Turner P. Feature extraction of wood-hole defects using empirical mode decomposition of ultrasonic signals. NDT & E International 2020;114:102282. doi:10.1016/j.ndteint.2020.102282.

[16] Wang L, Shao Y. Fault feature extraction of rotating machinery using a reweighted complete ensemble empirical mode decomposition with adaptive noise and demodulation analysis. Mechanical Systems and Signal Processing 2020;138:106545. doi:10.1016/j.ymssp.2019.106545.

[17] Au SK, Brownjohn JM, Li B, Raby A. Understanding and managing identification uncertainty of close modes in operational modal analysis. Mechanical Systems and Signal Processing 2021;147:107018. doi:10.1016/j.ymssp.2020.107018.

[18] Hassani S, Shadan F. Using incomplete frf measurements for damage detection of structures with closely-spaced eigenvalues. Measurement 2021;:110388doi:10.1016/j.measurement.2021.110388.

[19] Huang NE, Shen Z, Long SR, Wu MC, Shih HH, Zheng Q, et al. The empirical mode decomposition and the Hilbert spectrum for nonlinear and non-stationary time series analysis. Proceedings of the Royal Society of London A: Mathematical, Physical and Engineering Sciences 1998;454:903–95. doi:10.1098/rspa.1998.0193.

[20] Esfandiari A, Bakhtiari-Nejad F, Rahai A, Sanayei M. Structural model updating using frequency response function and quasi-linear sensitivity equation. Journal of sound and vibration 2009;326(3-5):557–73. doi:10.1016/j.jsv.2009.07.001.

[21] Shadan F, Khoshnoudian F, Esfandiari A. A frequency response-based structural damage identification using model updating method. Structural Control and Health Monitoring 2016;23(2):286–302. doi:10.1002/stc.1768.

[22] Yao X, Sun X, Yang Y, Wu D, Liang X. Features extraction and reconstruction of country risk based on empirical emd. Procedia Computer Science 2014;31:265–72. doi:10.1016/j.procs.2014.05.268.

[23] Muskhelishvili Nikolaĭ I, Radok JRM. Singular integral equations: boundary problems of function theory and their application to mathematical physics. Courier Corporation; 2008.

[24] Hildebrand FB. Advanced calculus for engineers. Prentice-Hall; 1949.

[25] Gabor D. Theory of communication. part 1: The analysis of information. Journal of the Institution of Electrical Engineers-Part III: Radio and Communication Engineering 1946;93(26):429–41.

[26] Boller C, Chang FK, Fujino Y. Encyclopedia of structural health monitoring. Wiley; 2009.

[27] Pines D, Salvino L. Structural health monitoring using empirical mode decomposition and the hilbert phase. Journal of sound and vibration 2006;294(1-2):97–124.

[28] Bernal D, Gunes B. An examination of instantaneous frequency as a damage detection tool. In: Proc. 14th Engineering Mechanics Conf. 2000,.

[29] Mousavi M, Gandomi AH. An input-output damage detection method using static equivalent formulation of dynamic vibration. Archives of Civil and Mechanical Engineering 2018;18:508–14. doi:10.1016/j.acme.2017.01.007.

[30] Mousavi M, Holloway D, Olivier J, Gandomi AH. A baseline-free damage detection method using vbi incomplete measurement data. Measurement 2021;174:108957.

[31] Pedram M, Esfandiari A, Khedmati MR. Finite element model updating using strain-based power spectral density for damage detection. Structural Control and Health Monitoring 2016;23(11):1314–33. doi:10.1002/stc.1833.

[32] Pereira J, Heylen W, Lammens S, Sas P. Influence of the number of frequency points and resonance frequencies on modal updating techniques for health condition monitoring and damage detection of flexible structure. In: Proceedings-SPIE The International Society for Optical Engineering. Citeseer; 1995, p. 1273–.

[33] Fathi A, Esfandiari A, Fadavie M, Mojtahedi A. Damage detection in an offshore platform using incomplete noisy frf data by a novel bayesian model updating method. Ocean Engineering 2020;217:108023. doi:10.1016/j.oceaneng.2020.108023.

[34] Dos Santos JA, Soares CM, Soares CM, Maia N. Structural damage identification in laminated structures using frf data. Composite Structures 2005;67(2):239–49. doi:10.1016/j.compstruct.2004.09.011.

[35] Reddy JN. Mechanics of laminated composite plates and shells: theory and analysis. CRC press; 2003.

[36] Nelson RB. Simplified calculation of eigenvector derivatives. AIAA journal 1976;14(9):1201–5. doi:10.2514/3.7211.

[37] Brincker R, Lopez-Aenlle M. Mode shape sensitivity of two closely spaced eigenvalues. Journal of Sound and Vibration 2015;334:377–87. doi:10.1016/j.jsv.2014.08.015.

[38] He WY, Ren WX, Zhu S. Damage detection of beam structures using quasi-static moving load induced displacement response. Engineering Structures 2017;145:70–82. doi:10.1016/j.engstruct.2017.05.009.

[39] Hassani S, Mousavi M, Gandomi AH. Damage detection of composite laminate structures using vmd of frf contaminated by high percentage of noise. Composite Structures 2022;:115243.

[40] Soh CK, Yang J. Fuzzy controlled genetic algorithm search for shape optimization. Journal of computing in civil engineering 1996;10(2):143–50. doi:10.1061/(ASCE)0887-3801(1996)10:2(143).

[41] Hassani S, Mousavi M, Gandomi AH. A mode shape sensitivity-based method for damage detection of structures with closely-spaced eigenvalues. Measurement 2022;:110644.